

THESIS

WHAT CONTROLS THE VARIABILITY OF OXYGEN
IN THE SUBPOLAR NORTH PACIFIC?

Submitted by

Yohei Takano

Department of Atmospheric Science

In partial fulfillment of the requirements

For the Degree of Master of Science

Colorado State University

Fort Collins, Colorado

Spring 2011

Master's Committee:

Advisor: Takamitsu Ito

David Thompson

John Harton

Curtis Deutsch

Copyright by Yohei Takano 2011

All Rights Reserved

ABSTRACT OF THESIS

WHAT CONTROLS THE VARIABILITY OF OXYGEN
IN THE SUBPOLAR NORTH PACIFIC?

Dissolved oxygen is a widely observed chemical quantity in the oceans along with temperature and salinity. Changes in the dissolved oxygen have been observed over the world oceans. Observed oxygen in the Ocean Station Papa (OSP, 50°N, 145°W) in the Gulf of Alaska exhibits strong variability over interannual and decadal timescales, however, the mechanisms driving the observed variability are not yet fully understood. Furthermore, irregular sampling frequency and relatively short record length make it difficult to detect a low-frequency variability. Motivated by these observations, we investigate the mechanisms driving the low-frequency variability of oxygen in the subpolar North Pacific. The specific purposes of this study are 1) to evaluate the robustness of the observed low-frequency variability of dissolved oxygen and 2) to determine the mechanisms driving the observed variability using statistical data analysis and numerical simulations.

To evaluate the robustness of the low-frequency variability, we conducted spectral analyses on the observed oxygen at OSP. To address the irregular sampling frequency we randomly sub-sampled the raw data to form 500 ensemble members with a regular time interval, and then performed spectral analyses. The resulting power spectrum

of oxygen exhibits a robust low-frequency variability and a statistically significant spectral peak is identified at a timescale of 15-20 years.

The wintertime oceanic barotropic streamfunction is significantly correlated with the observed oxygen anomaly at OSP with a north-south dipole structure over the North Pacific. We hypothesize that the observed low-frequency variability is primarily driven by the variability of large-scale ocean circulation in the North Pacific. To test this hypothesis, we simulate the three-dimensional distribution of oxygen anomaly between 1952 to 2001 using data-constrained circulation fields. The simulated oxygen anomaly shows an outstanding variability in the Gulf of Alaska, showing that this region is a hotspot of oxygen fluctuation. Anomalous advection acting on the climatological mean oxygen gradient is the source of oxygen variability in this simulation. Empirical Orthogonal Function (EOF) analyses of the simulated oxygen show that the two dominant modes of the oxygen anomaly explains more than 50% of oxygen variance over the North Pacific, that are closely related to the dominant modes of climate variability in the North Pacific (Pacific Decadal Oscillation and North Pacific Oscillation). Our results imply the important link between large-scale climate fluctuations, ocean circulation and biogeochemical tracers in the North Pacific.

ACKNOWLEDGEMENTS

First I would particularly like to thank my advisor, Professor Takamitsu Ito for his guidance and support for the past two and half years. His patience and support for graduate study in both research and graduate school life in abroad helped me a lot. I cannot thank him enough for all the support. I would also like to thank my committee members Dr. David Thompson, Dr. Curtis Deutsch and Dr. John Harton for helpful discussions and all the support in course work.

Members in Ocean and Climate research group encouraged me a lot through my graduate work. I would like to say thank you to all the members and friends in graduate school.

Finally I would like to thank my family and friends in Japan for all the support. This work has been supported by the National Science Foundation (NSF). (Grant number OCE-0851497).

TABLE OF CONTENTS

ABSTRACT	ii
ACKNOWLEDGEMENT	iv
TABLE OF CONTENTS	v
1. INTRODUCTION	1
1-1. Background: Dissolved Oxygen in the Oceans	1
1-2. Observed Oxygen and Climate Variability of the North Pacific	5
1-3. Ocean Station Papa	13
1-4. Objective of this Thesis	16
2. TIME SERIES ANALYSIS OF OBSERVED OXYGEN	18
2-1. Background	18
2-2. Methods	20
2-3. Results: Fundamental Statistical Properties	22
2-4. Results: Spectral Analysis	31
2-5. Summary and Discussion	37
3. MODELING THE LOW FREQUENCY VARIABILITY OF OXYGEN IN THE NORTH PACIFIC	39
3-1. Background	39
3-2. North Pacific Circulation and Thermocline Oxygen	40
3-3. Hypothesis	47

3-4. A Three Dimensional Simulation of Oxygen Anomaly	49
3-5. Climate-driven Oxygen Anomaly	53
3-6. Summary and Discussion	59
4. CONCLUSION	61
BIBLIOGRAPHY	65

CHAPTER 1. INTRODUCTION

1-1. Background: Dissolved Oxygen in the Oceans

Dissolved oxygen in the ocean is the third most frequently observed ocean tracer following temperature and salinity. Oxygen reflects both physical and biological processes in the oceans and can be measured accurately from the in situ water samples.

Oxygen is essential for life, and various organisms adapt to a wide range of oxic conditions. Some organisms require well-oxygenated conditions (for their rapid metabolism), while others tolerate brief periods of low-oxygen conditions (Davis, 1975; Gray et al., 2002). Hypoxic ($O_2 < 60 \mu\text{mol/kg}$) and anoxic ($O_2 \sim 0 \mu\text{mol/kg}$) events can substantially impact on ecosystem and fisheries. Oxygen concentration controls a suite of chemical reactions and biological activity (such as remineralization, transformations of organic molecules to inorganic forms) in the seawater and sediment. The volume of hypoxic water impacts on the nitrogen budget and the global nutrient inventory. Furthermore, the oceanic oxygen budget influences the interpretation of atmospheric oxygen and the partitioning of carbon uptake between lands and oceans. Changes in dissolved oxygen can also be used to detect and interpret the response of ocean circulation and biogeochemistry to climate change.

Oxygen distribution in the oceans is mainly controlled by three mechanisms: 1) air-sea gas exchange, 2) transport by ocean circulation, and 3) biological sources and sinks as shown in the schematic diagram below (Figure 1-1).

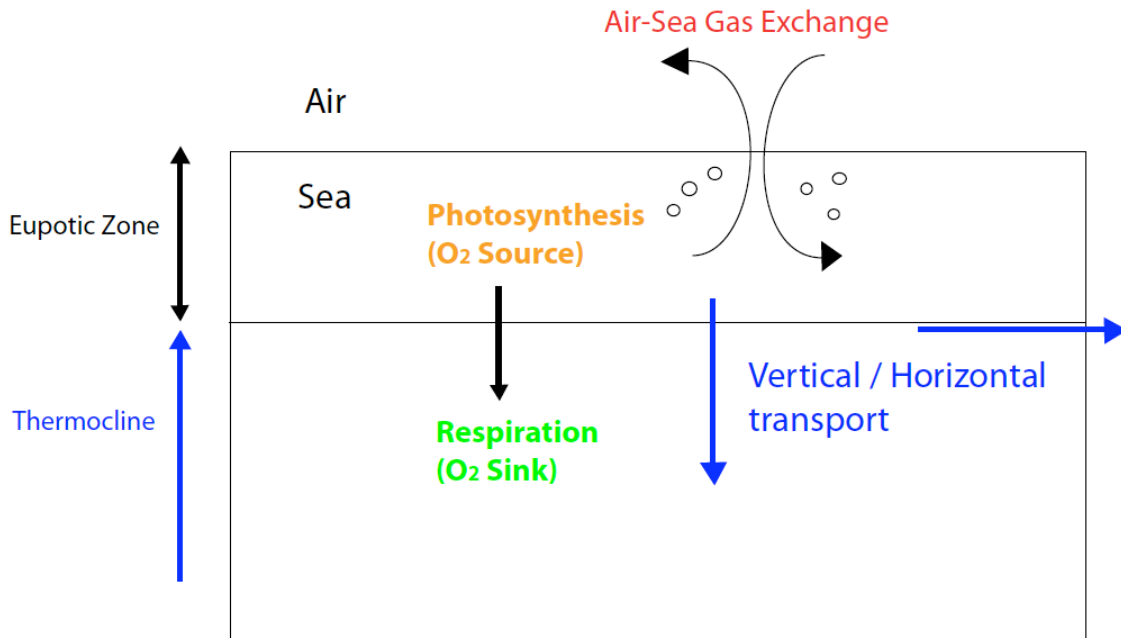


Figure 1-1. Schematic diagram of processes how oxygen variability is controlled.

1) Oxygen accounts for approximately 20% of atmospheric composition, and air-sea gas exchange tends to keep surface waters very close to saturation with overlying atmospheric oxygen. Surface oxygen can be controlled by the saturated oxygen concentration at local temperature and salinity, and by the degree of equilibration attained through gas-exchange with the atmosphere (Ito et al., 2004). The oxygen-rich surface water can then be physically transported into the interior ocean.

2) Transport by ocean circulation includes both horizontal circulation and ventilation (vertical transport). Horizontal circulation (such as gyre circulation) can redistribute oxygen over long distances. Ventilation (subduction) of water masses carries the oxygen-rich surface waters down into the interior ocean.

3) Photosynthesis by phytoplankton produces oxygen in the surface ocean, which tends to supersaturate surface oxygen concentration. Subduction of the oxygen-rich surface water brings oxygen from the surface to the interior ocean. As the water travels in the interior thermocline, oxygen is slowly consumed by the decomposition of organic material, and thus the deep waters are relatively depleted in oxygen. These biological processes tend to generate a vertical gradient of oxygen.

First we will glance the climatology of oxygen distribution over the North Pacific. Figure 1-2 shows the climatological distribution of oxygen along the three constant density surfaces (isopycnal), potential density (σ_θ) = 26.0, 26.5 and 27.0 based on World Ocean Atlas 2005 (Garcia et al., 2006). There is a large (O (1)) spatial gradient of oxygen in the mean state. Fluctuations in ocean circulation can act on this background oxygen gradient to generate significant variability. In the deepest specific density layer ($\sigma_\theta = 27.0$), newly ventilated waters in the Sea of Okhotsk are enriched in oxygen, and the high oxygen spreads from the western to central Pacific. There is a general north-south gradient of oxygen at all density levels contrasting the well-ventilated subtropical waters and poorly ventilated tropical thermocline. Oxygen concentration is also higher near the surface, and it decreases downward in the top several hundreds of meters of the upper ocean.

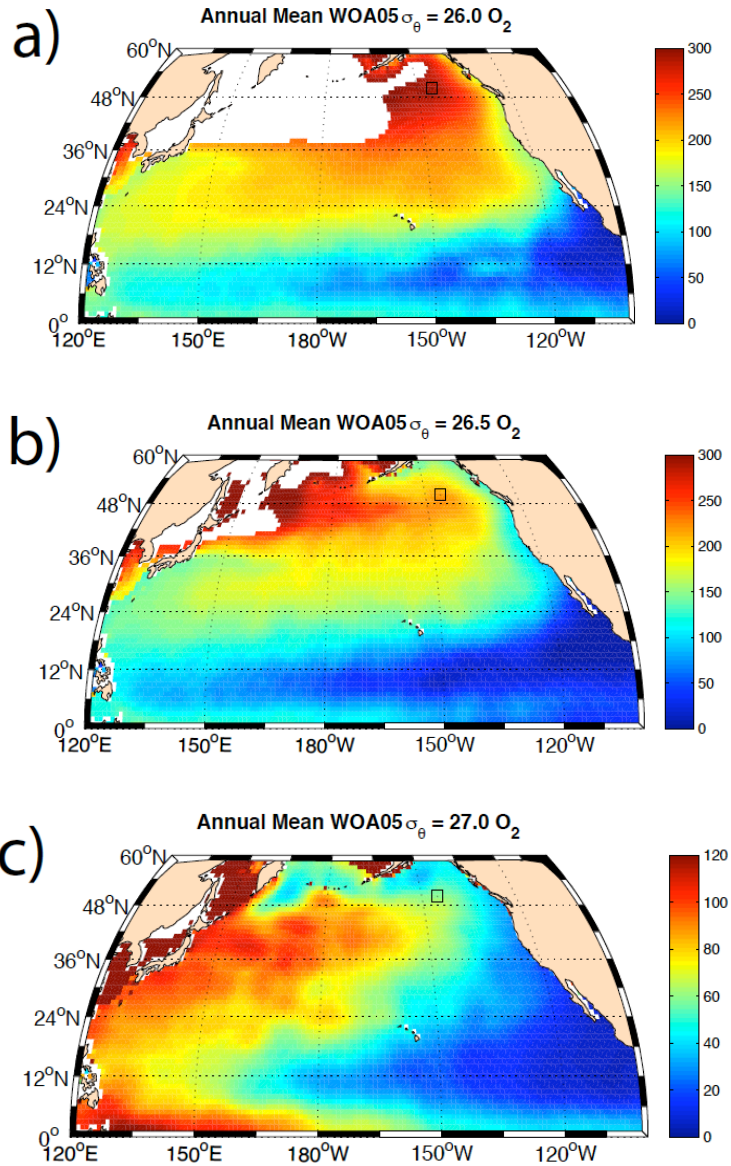


Figure 1-2. Annual mean climatology of oxygen concentration (from World Ocean Atlas 2005) over the North Pacific three isopycnal surfaces at $\sigma_\theta =$ (a) 26.0 (b) 26.5 and (c) 27.0. The locations of the Ocean Station Papa are shown in black box. The regions where isopycnal layer depth less than 5m are extracted. Units are in [$\mu\text{mol/kg}$].

1-2. Observed Oxygen and Climate Variability of the North Pacific

Changes in dissolved oxygen concentration have been observed across major ocean basins (Keeling and Garcia, 2002; Keeling et al., 2010), which may be due to the responses of ocean circulation and biology to climate variability. Oxygen concentration can be sensitive to anthropogenic climate change, as the heating of the oceans decreases the solubility of oxygen, and increasing thermal stratification may prevent the oxygen-rich surface waters to subduct into the thermocline. Oxygen variability in the North Pacific has been analyzed using observations and numerical models (Ono et al., 2001; Emerson et al., 2004; Deutsch et al., 2005, 2006; Watanabe et al., 2008).

The subarctic North Pacific contains two of the longest time series of oxygen measurements in the western (Oyashio region) and eastern (Gulf of Alaska) part of the basin (Ono et al., 2001; Whitney et al., 2007). Analyzing 30-year time series of observational data in the Oyashio region, Ono et al., (2001) showed a decreasing, long-term trend in oxygen superimposed with more energetic decadal variability. Observed low-frequency variability in the subsurface oxygen is correlated with the Aleutian Low activity (correlation coefficient is -0.88, Ono et al., 2001). Watanabe et al., (2008) analyzed additional time series data in the subpolar North Pacific, and suggested that variability of oxygen and nutrients in the eastern (Gulf of Alaska) and western (Oyashio) time series are related. Linear trends as well as decadal variability are significant in the observed oxygen and nutrients, and the observed decadal variability is of opposite phases between the western and eastern part of the basin (see figure 1-3).

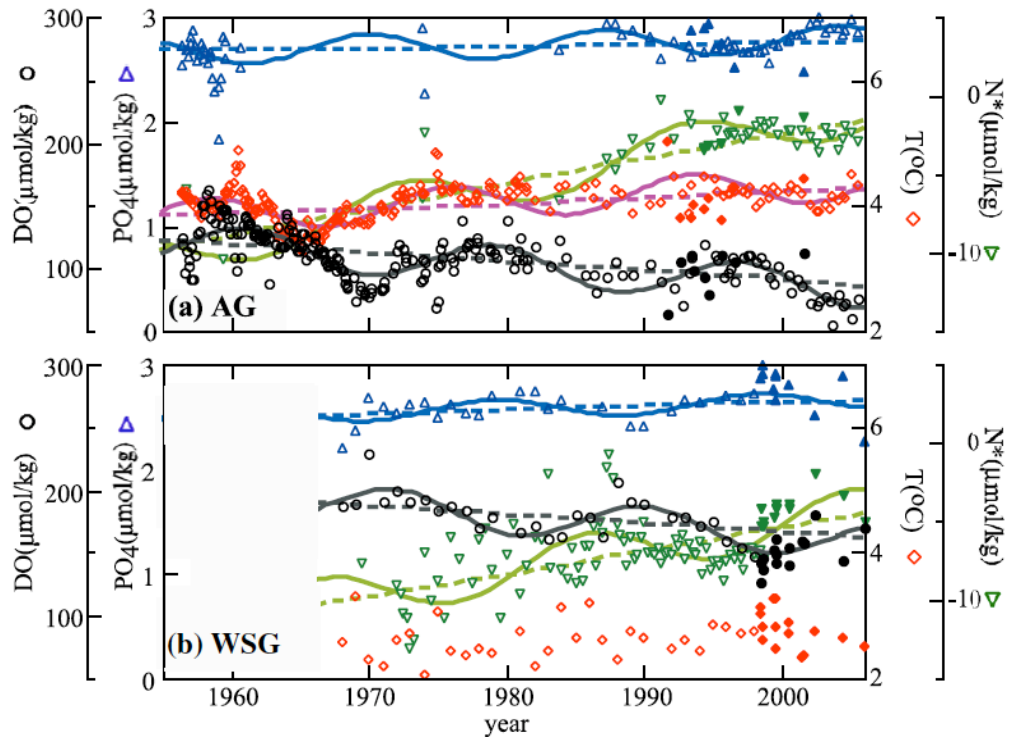


Figure 1-3. Observed time series of dissolved oxygen (black circle), PO_4 (blue triangle) temperature (red diamond) and N (green triangle) in the subsurface ocean cited from Watanabe et al., (2008). Solid and dashed line indicates fitted curves and linear trends. (a) Time series on $\sigma_\theta = 26.8$ at Gulf of Alaska and (b) Western Subarctic Gyre.

Deutsch et al., (2005, 2006) investigated the temporal variability of oxygen in the upper water column of the North Pacific using an isopycnal circulation model including a simple parameterization of biogeochemical cycle (Najjar et al, 1992). In consistency with the observation, the simulation reproduced a decreasing oxygen trend in the lower ventilated thermocline at subpolar latitudes, and increasing oxygen in much of the subtropics over the time period of 1980s and 1990s. Sensitivity experiments show that physical transport of oxygen is the dominant cause of simulated oxygen variability in the

North Pacific, indicating that oxygen could be used as a tracer of physical circulation variability in the region (see figure 1-4).

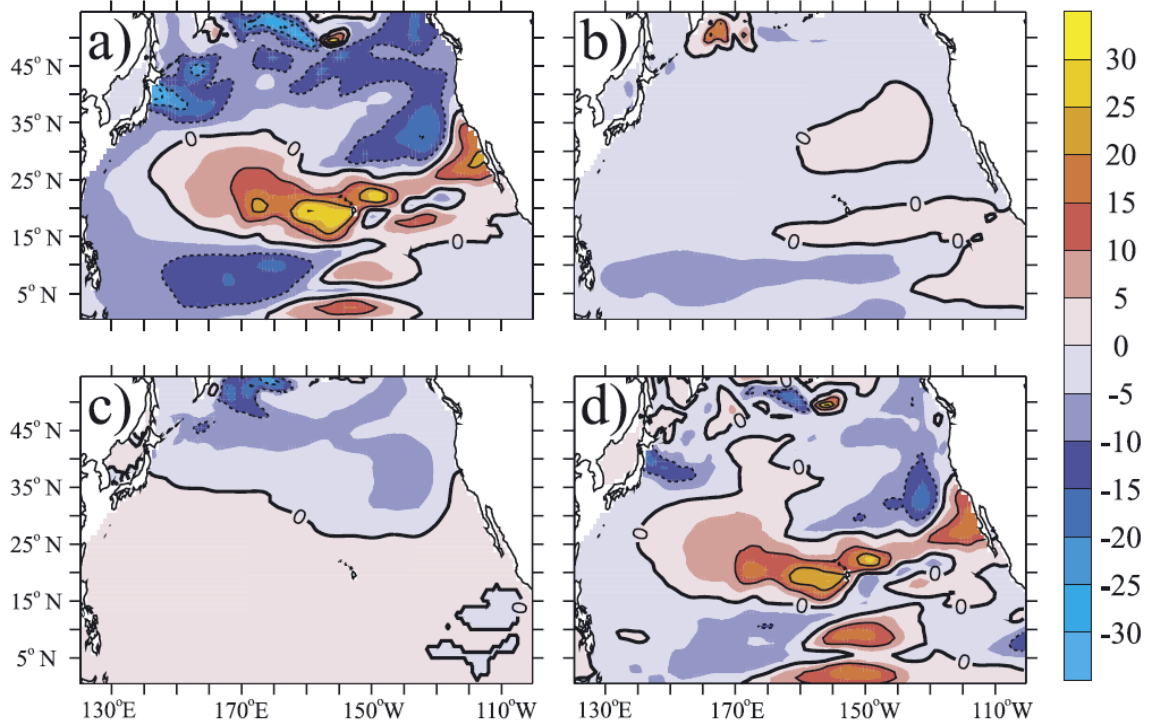


Figure 1-4. Difference between decadal mean O₂ (μmol/kg) in the 1990s and the 1980s along the isopycnal surface ($\sigma_{\theta} = 26.8$) from Deutsch et al., (2006). The (a) total O₂ difference is the sum of O₂ anomalies due to (b) biological changes, (c) ventilation changes and (d) changes in circulation.

What controls the decadal variability of oxygen and other biogeochemical tracers in the North Pacific? Recently Di Lorenzo et al., (2008) defined a regional mode of variability in the northeastern Pacific, the North Pacific Gyre Oscillation (NPGO) based on the Empirical Orthogonal Function (EOF) of the dynamic sea-surface height anomalies (SSHa) in the northeastern Pacific (180°W-110°W; 25°N-62°N). The first principal component (PC) is the regional representation of the Pacific Decadal Oscillation

(PDO, Mantua et al., 1997), and the second PC is the NPGO mode. The PDO mode shows a single large gyre north of 25°N and an anomalously strong poleward flow along the entire coast from 25°N to 55°N (see figure 1-5 left panels). In contrast, the NPGO mode in its positive phase shows a pair of counter-rotating gyres that reflect the gyre-scale mean geostrophic circulation (see figure 1-5 right panels).

The NPGO variability is significantly correlated with observed sea surface temperature (SSTa), salinity (SSSa), nutrients, chlorophyll (Chl-a) and oxygen of the northeastern Pacific along the coast of California (see Table 1-1). While the sea surface temperature is more strongly correlated with the PDO mode, sea surface salinity and other biogeochemical tracers including oxygen are more strongly correlated with the NPGO mode. The associated changes in the wind forcing and sea level pressure pattern with PDO mode and NPGO mode are shown in figure 1-6. When the NPGO is positive, the associated changes in wind forcing create upwelling-favorable conditions in the California current and Alaskan Gyre, but downwelling condition in the Subtropical Gyre and the Alaskan Coastal Current (Di Lorenzo et al., 2008). The anomalous upwelling associated with the NPGO mode can bring up oxygen-depleted and nutrient-enriched thermocline waters in the California coast.

Table 1-1

	PDO	NPGO
SSTa	0.44	0.29
SSSa	0.06	0.42
Chl-a	0.21	0.47
NO ₃	0.26	0.51
PO ₄	0.19	0.35
SiO ₄	0.31	0.53
O ₂	0	-0.50

Correlations of the Model PDO and NPGO indices with CalCOFI (California Cooperative Oceanic Fisheries Investigation) data cited from Di Lorenzo et al., (2008). The time series of SSTa, SSSa and Chl-a are averages of surface observations from the CalCOFI program in the Southern California Current. The nutrient time series are spatial averages of samples from 150m depth. Bold numbers indicate correlation significant at the 95% level or higher.

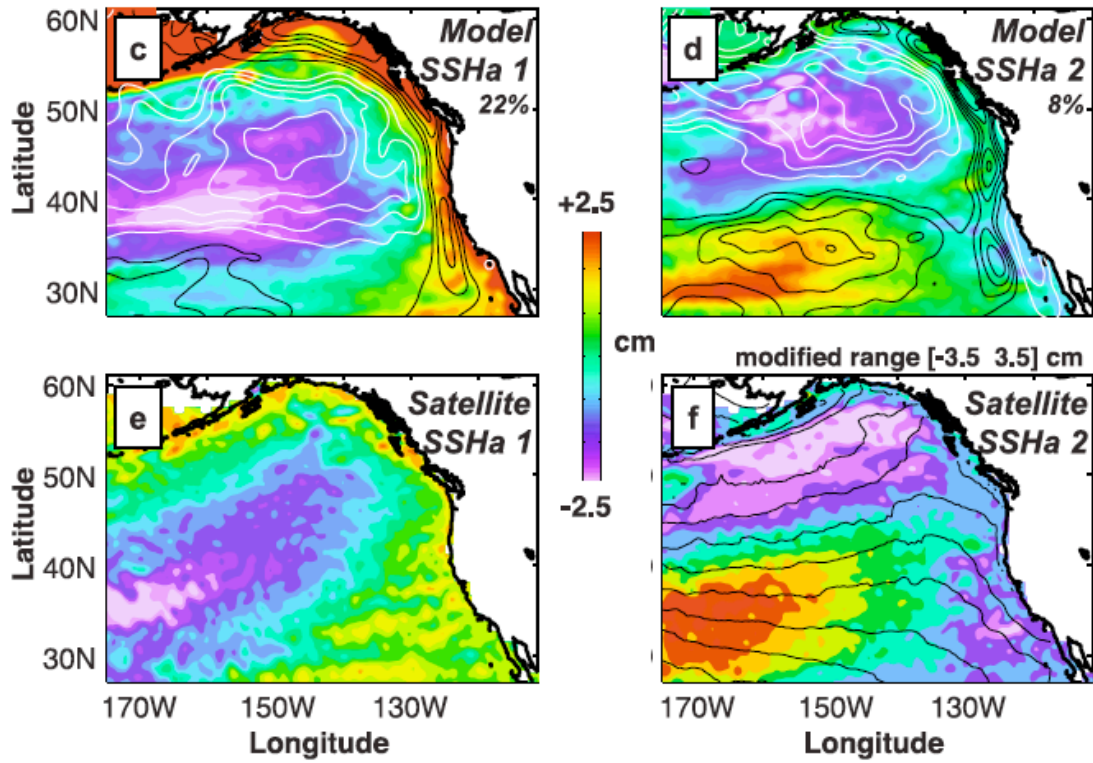


Figure 1-5. PDO and NPGO patterns in sea surface height field based on model and data (from Di Lorenzo et al., 2008). Left panels show the PDO pattern and right panels show the NPGO pattern.

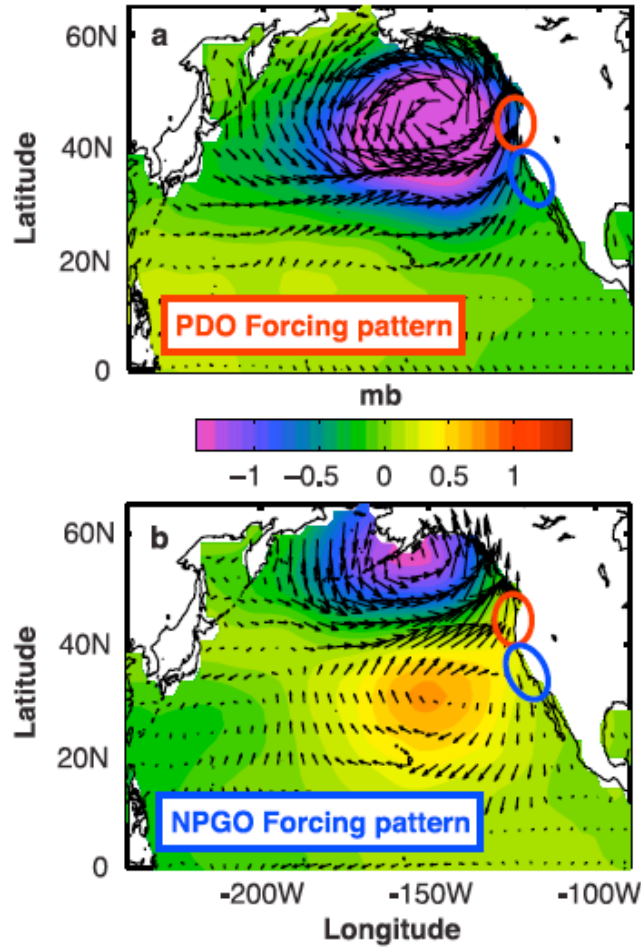


Figure 1-6. Regression maps of (a) PDO and (b) NPGO indices with NCEP windstress vectors and sea level pressure (color scale) (cited from Di Lorenzo et al., 2008).

The spatial structure of the wind stress anomalies associated with NPGO is similar to the positive phase of the North Pacific Oscillation (NPO) / West Pacific (WP) pattern (Walker and Bliss, 1932; Linkin and Nigam, 2008), which is the second PC of the atmospheric sea level pressure and geopotential height in the extratropical North Pacific (figure 1-7). Associated SST and surface wind pattern are shown in figure 1-8. The SST signal is apparently wind driven: In the tropics, the NPO/WP wind anomalies, especially anticyclonic flow around the southern cell, intensifies the trades in the central/eastern

basin and weakens westerlies in the subtropical western basin, while cyclonic flow about the northern cell strengthens the midlatitude westerlies. The resulting wind speed and surface fluxes - stronger in the trade wind zone and weaker in the subtropics - lead to SST changes (Linkin and Nigam, 2008). However, the NPO/WP influence on SST is not very strong based on the correlation map (maximum correlations are ~ 0.3).

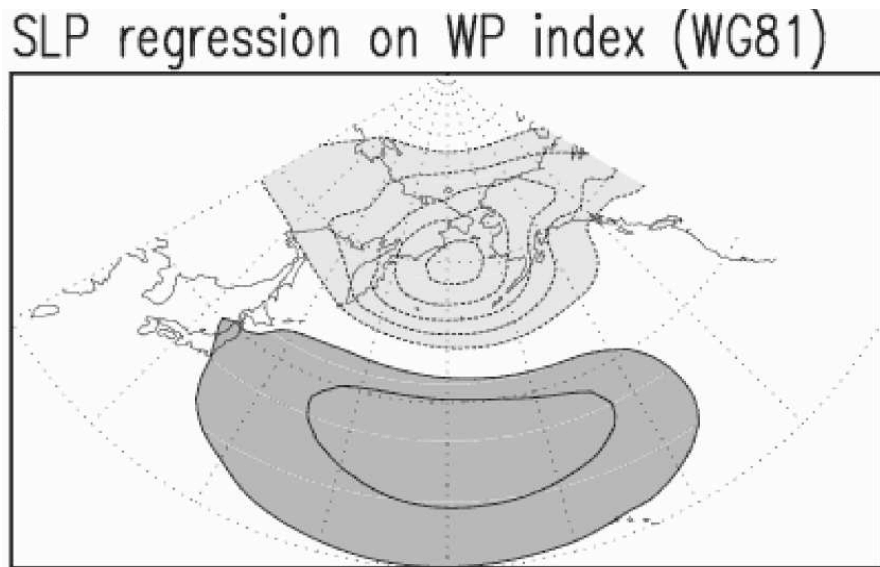


Figure 1-7. Regression maps of NPO/WP index with winter SLP in the Pacific sector (cited from Linkin and Nigam, 2008). Solid (dashed) contours denote positive (negative) values: the contour lines with zeros are suppressed.

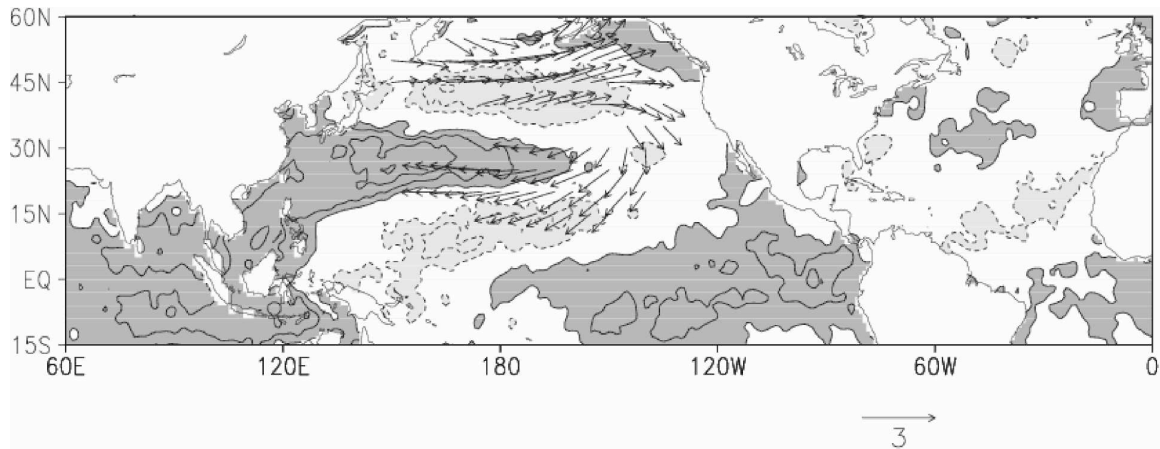


Figure 1-8. NPO/WP SST correlations and 1000-hPa wind regressions during 1958-2001 winter months (cited from Linkin and Nigam, 2008). SST is from HadISST dataset while winds are from ERA-40. Solid (dashed) contours denote positive (negative) values.

1-3. Ocean Station Papa

The longest record of dissolved oxygen in the subpolar North Pacific comes from the Gulf of Alaska, Ocean Station Papa (OSP, 50°N, 145°W, see figure 1-9). OSP measurements were initially established by a weathership in December 1949, and then routine oceanographic measurements have been continuously performed until today with varying sampling frequency (Ocean Station Papa website: <http://www.pmel.noaa.gov/stnP/overview.html>).

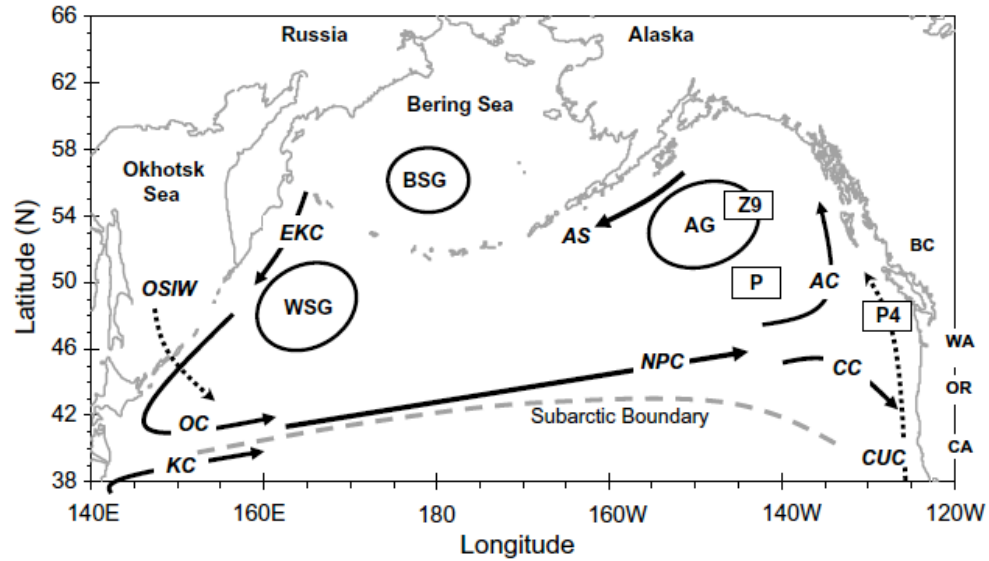


Figure 1-9. Map of the North Pacific Ocean showing major currents (cited from Whitney et al., 2007). Label P shows the location of Ocean Station Papa (P) at 50°N, 145°W.

Over fifty years of time series measurements of oceanic physical properties are available at OSP. Cummins and Lagerloef, [2002] examined the low-frequency variability of the depth of the main pycnocline (a layer where the density increases rapidly with depth), demonstrating that a large fraction (about 50%) of the low-frequency variability in the depth of the pycnocline at OSP could be well explained by the local Ekman pumping. Through this mechanism, the PDO and associated wind stress curl have a large influence on the pycnocline variability at OSP.

Based on the observed hydrographic and oxygen data between 1956 and 2006, Whitney et al., [2007] found waters below the ocean mixed layer depth to at least 1000m have been warming and losing oxygen over the last 50 years. However, decadal fluctuations are much stronger than the long-term trend in the oxygen data as shown in figure 1-10, and it is not yet clear what controls this variability.

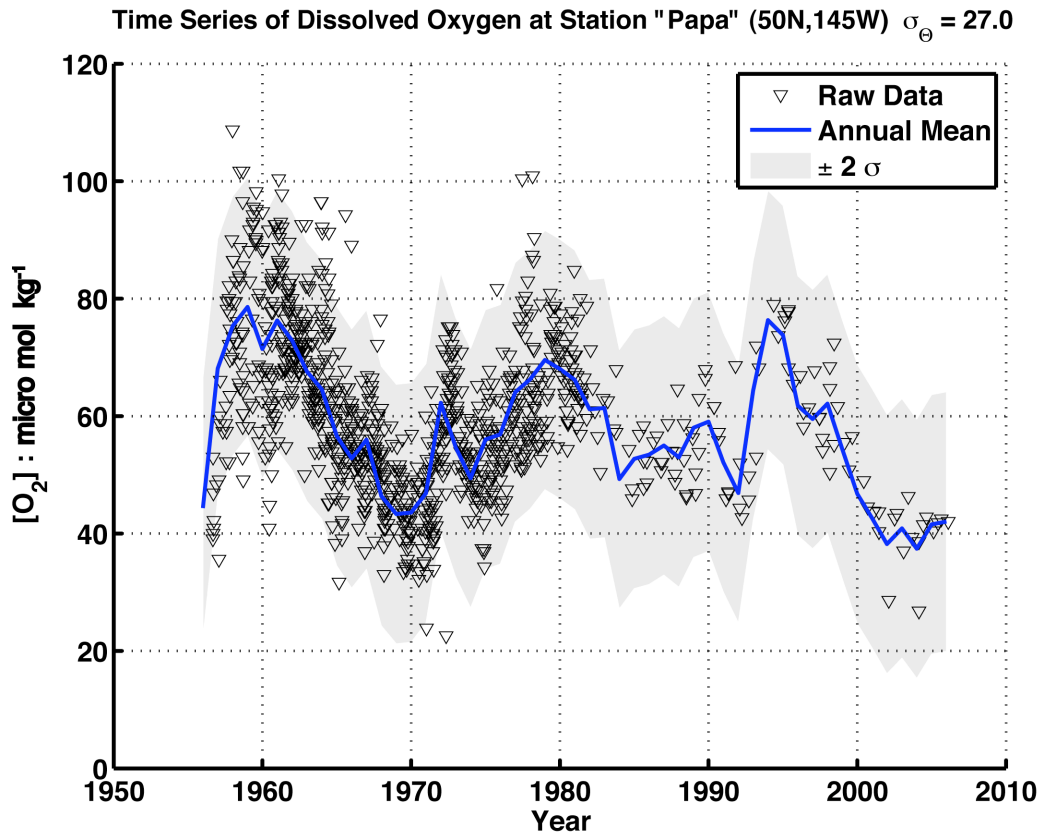


Figure 1-10. Observed isopycnal ($\sigma_{\theta} = 27.0$) dissolved oxygen at OSP. Triangle shows the raw data of dissolved oxygen.

Motivated by the outstanding low-frequency variability of oxygen at OSP, Ito and Deutsch, (2010) developed a conceptual model to illustrate mechanisms controlling the low-frequency variability of thermocline oxygen. The model is analogous to the stochastic climate model of Hasselmann (1976) where the negative feedback of air-sea heat fluxes is replaced by the flushing effect of thermocline ventilation. The ventilation of thermocline naturally integrates the effects of anomalous respiration and advection over the decadal timescales, so short-lived oxygen perturbations are strongly damped, producing a red spectrum of oxygen variance. The model was then applied to the

observed thermocline oxygen at OSP, and found a statistically significant spectral peak at the 15-20 year timescale. While their analysis shows the significance of the low-frequency variability in this region, it is not clear what physical and biogeochemical processes can cause the decadal timescale fluctuation of oxygen.

1-4. Objectives of this Thesis

Figure 1-10 clearly demonstrates the dynamic variability of dissolved oxygen in the subpolar Pacific. Observed oxygen variability is correlated with the NPGO in interannual and decadal timescales (correlation coefficient is -0.64, significant at 95% level), however, the mechanistic links between physical climate variability and biogeochemical tracers are not yet understood. Previous studies identified the increased variance of oxygen in the 15-20 year timescale, but it is not clear what sets this timescale. Furthermore, the irregular sampling frequency and relatively short length of the time series data make it difficult to detect the low-frequency variability in a robust way.

The main objective of this study is to better understand the mechanisms controlling the observed oxygen variability in the main thermocline of the subpolar North Pacific. In particular, we focus on the density range of North Pacific Intermediate Water (NPIW, isopycnal layer at $\sigma_{\theta} = 27.0$). This isopycnal layer is below the base of the euphotic zone and winter mixed-layer, so there is no direct influence from the surface processes. The following two questions are addressed in this thesis:

- 1) **How robust is the low-frequency variability of thermocline oxygen at OSP?**
- 2) **What causes the observed thermocline oxygen variability?**

These two questions are addressed in the following two chapters. Chapter 2 focuses on the time-series analysis of oxygen observation at OSP. In order to quantify and establish the robustness of the low frequency variability, detailed statistical analyses are performed. Chapter 3 focuses on the mechanism of oxygen variability in the subpolar North Pacific, employing two complementary approaches. First, correlation and regression analyses are performed to indentify links between observed oxygen and physical properties. Then, a numerical ocean model is used to simulate the oxygen variability. The model fields are first tested against the observational data, and EOF analyses are performed to extract the modes of oxygen variability.

CHAPTER 2. TIME SERIES ANALYSIS OF OBSERVED OXYGEN

2-1. Background

Dissolved oxygen in the thermocline of the subpolar North Pacific shows a strong decadal variability. The low-frequency variability of oxygen is particularly interesting as it may reflect the effect of low frequency variability in physical and biogeochemical processes. One of the longest ocean time series observations of dissolved oxygen comes from the North Pacific. Time series measurements at Ocean Station Papa (OSP, 50°N, 145°W) and the ocean transect Line P (Figure 9, in Chapter 1) has been operating since 1949. Ito and Deutsch, (2010) have analyzed 51-year long (between 1956 – 2006) oxygen time series data at OSP below the base of winter mixed layer on the isopycnal surface $\sigma_{\theta} = 27.0$ which is about 350 – 400m depth. Below the base of winter mixed layer, the seawater cannot directly interact with overlying atmosphere through seasonal convection. Therefore the variability of oxygen at this density level is likely influenced by processes occurring in the interior ocean including ocean circulation and biological respiration.

Taking advantage of the relatively long time series at OSP, Ito and Deutsch (2010) performed a spectral analysis, finding a low-frequency variability with a statistically significant spectral peak at the 15-20 year timescale. As they discussed, there are some caveats in this study. First, the timescale of 15-20 years is comparable to the

length of the time series data itself, only allowing 2 to 3 cycles of this variability, making it difficult to determine the statistical significance of the signal. Secondly, the sampling frequency has changed significantly before and after 1981. Between December 1949 and June 1981, OSP has been operating as an ocean weather station where large number of water samples has been taken until the end of 1970s. During this period, the water samples are taken on weekly timescale. After 1981, observations are continued by the Institute of Ocean Science (IOS) and the number of water samples dramatically decreased to about 3-6 samples per year (Whitney and Freeland, 1999, Whitney et al., 2007). This sudden decrease in sampling density is concerning as we interpret the spectral analysis of Ito and Deutsch (2010) in which the Fourier analysis is applied to the annually binned time series data without specific treatment for the shift in sampling frequency. Thirdly, based on the limited data before 1980s, there is a significant intra-annual and inter-annual variability of oxygen at OSP. This is unlikely a simple artifact of sampling error, and this high-frequency variability may not be well sampled enough after 1980s. Even though these measurements are taken below the base of the winter mixed layer, there could be episodic export of organic material, mesoscale eddy variability and other processes that can introduce such high-frequency variability, which is not taken into account in the previous studies where the data is simply averaged annually. These outstanding issues motivate further investigations to address several scientific questions.

- **How can we establish the statistics of oxygen time series with irregular sampling frequency?**
- **How robust is the low-frequency variability of oxygen at OSP?**

- **Can we determine statistical significance of the spectral peak in the 15-20 year timescale?**

In this chapter, we revisit the time series analysis of dissolved oxygen at OSP to resolve above questions. The organization of the chapter is as follows. In the following section we will describe the method of time series analysis. To address the irregular sampling frequency and to clarify the low-frequency variability, we analyzed the time series data at OSP with an improved statistical methods. As we discuss below, our analysis includes random sampling of the raw data with minimal averaging before performing spectral analysis. This approach is applied not only to oxygen but also temperature and salinity of the isopycnal surface ($\sigma_{\theta} = 27.0$). In section 2-3, fundamental statistical properties are briefly explained. In section 2-4, results from spectral analysis based on ensemble members are described and finally in section 2-5, we summarize and discuss the implication of our results.

2-2. Methods

In this section, we describe the improved method of time series analysis, which addresses the issues of irregular sampling. Observed oxygen data at OSP on the isopycnal surface, $\sigma_{\theta} = 27.0$, has a total of 1037 data points between 1956 and 2006. However, these data points are not distributed uniformly in time. Before 1981, there are over 30 data points per year. After 1981, the sampling frequency becomes about 5 data points per

year. Previous study of Ito and Deutsch (2010) simply binned the data annually and made an annual mean time series.

A new approach is developed to perform time series analyses of the OSP data without making excessive averaging of the raw data. To achieve this goal, we first randomly sample 200 data points from all the data, including 120 samples from the period of 1956 – 1980 and 80 samples from the period of 1981 – 2006. This sub-sampling of the data is separately performed between the two periods due to the different data density. While this operation reduces the total number of data points in the sub-sampled time series, the irregularity in the data density is effectively removed. Then the 200 data points are binned annually to form an annual time series over the 51-year period. On average, there are about 4 data points per year, and we discard cases with a missing year. This sampling scheme is repeated numerous times by a computer program to generate 500 ensemble members. This operation is also carried out for the temperature, and salinity on the isopycnal surface. This new approach enables us to retain information in the original dataset as much as possible while effectively removing the irregular data density.

Once the ensemble members are established, we performed the basic statistical analysis including the mean, standard deviation and effective sample size of each ensemble members. The effective sample size is calculated following the method developed by Bretherton et al., (1999).

$$N^* = N \frac{1 - r^2}{1 + r^2} \quad (2-1)$$

N is the number of the samples and r is the lag-one auto-correlation for the time series. The e-folding timescales are also calculated from the lag-one autocorrelation.

2-3. Result: Fundamental Statistical Properties

In this section, basic statistical properties are presented from the ensemble members. Figure 2-1 shows the annually binned time series data using all the observations. Similar plot is generated based on the ensemble mean time series in figure 2-2. The three panels show oxygen, temperature and salinity data. Ensemble means are calculated from simply taking an average of 500 ensemble members for each year. The shaded areas in Figure 2-1 and 2-2 show the spread of data with two standard deviations. Correlation coefficients between annually binned and ensemble mean data are 0.99 for all tracers indicating that annually binned and ensemble mean time series are essentially the same. Basic statistics are identical between annually binned and ensemble mean data because they come from the same time series, and large enough ensemble members have been included.

Visual inspection of the time series data suggest that the annually binned and ensemble mean data contain some low-frequency (decadal) variability. Also salinity data seems to contain significant high-frequency (interannual) variability relative to the oxygen concentration and temperature. Linear trend lines are also plotted where moderate long-term trends are found in all data. Temperature is warming, and oxygen is declining in the thermocline as previously discussed in Whitney et al., (2007). Temperature increased about 0.25 °C while dissolved oxygen decreased about 10 $\mu\text{mol/kg}$ between 1956 - 2001. The effect of temperature increase on the solubility of oxygen can explain about 1.5 $\mu\text{mol/kg}$ decrease in the oxygen concentration, which is only about 15% of the observed long-term change. The direct effect of heating alone cannot explain the long-

term trend in the dissolved oxygen during this period. The salinity increased about 0.05 psu during this period, which has almost no impact on the solubility of oxygen. This indicates that some other mechanism must play the dominant role in the long-term loss of oxygen from this region.

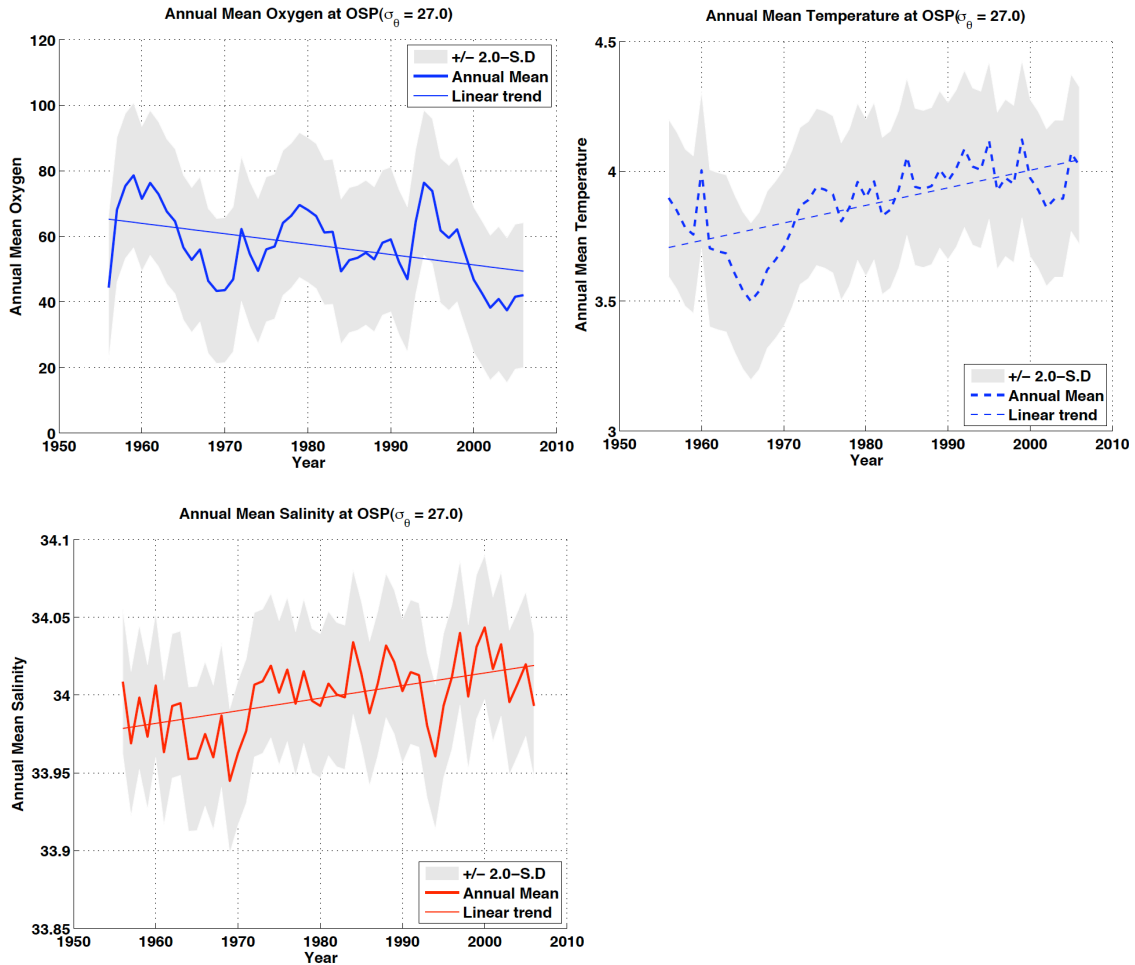


Figure 2-1. The annual mean isopycnal ($\sigma_\theta = 27.0$) dissolved oxygen concentration, temperature and salinity at OSP from 1956 -2006. Annual means are calculated from all the observational data. The linear trend lines are also plotted in the same figures.

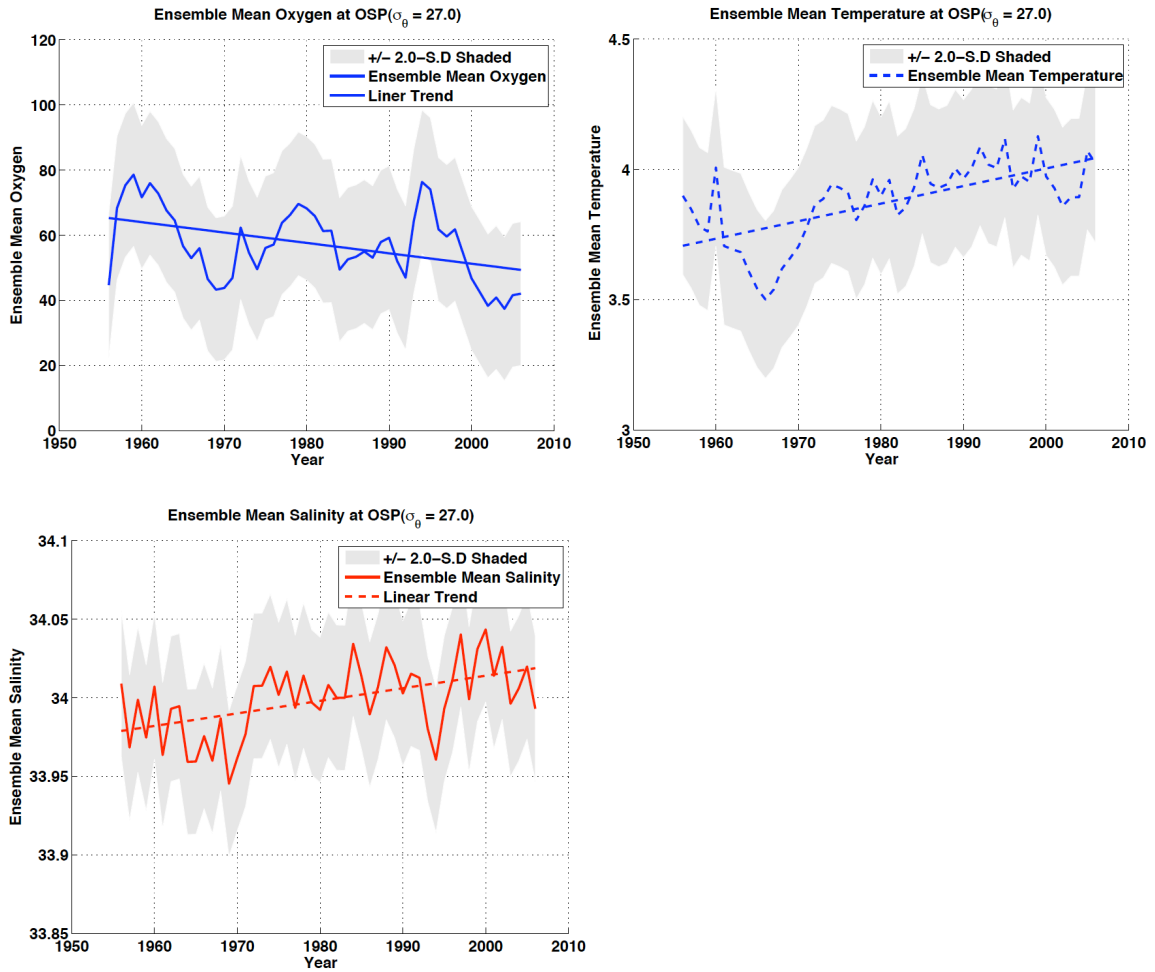


Figure 2-2. The same as in figure 2-1 except for ensemble mean isopycnal oxygen concentration, temperature, salinity and isopycnal depth. Ensemble means are calculated from simply taking an average of 500 ensemble members for each year.

Correlation coefficients between annual mean indices and linear trend lines are 0.43(for oxygen), 0.67(for temperature) and 0.52(for salinity) respectively, indicating that 16-36% of the variance of the observed physical properties at OSP could be explained by the trend. The strongest trend is in the temperature variability (about 36% of the variance). For oxygen, about 16% of variance is explained by the linear trend. This indicates that the long-term trend in oxygen concentration is relatively weak compared to

the interannual and decadal variability. This motivates us to examine the interannual and decadal variability, which will be the focus of the rest of this study.

Detrended time series data are also plotted in figure 2-3 based on the ensemble mean. Linear trend is removed from the original time series focusing on the variability, leaving the interannual and decadal variability. The variability in the dissolved oxygen and temperature are similar (contains low-frequency variability) compared to the salinity (contains high-frequency variability).

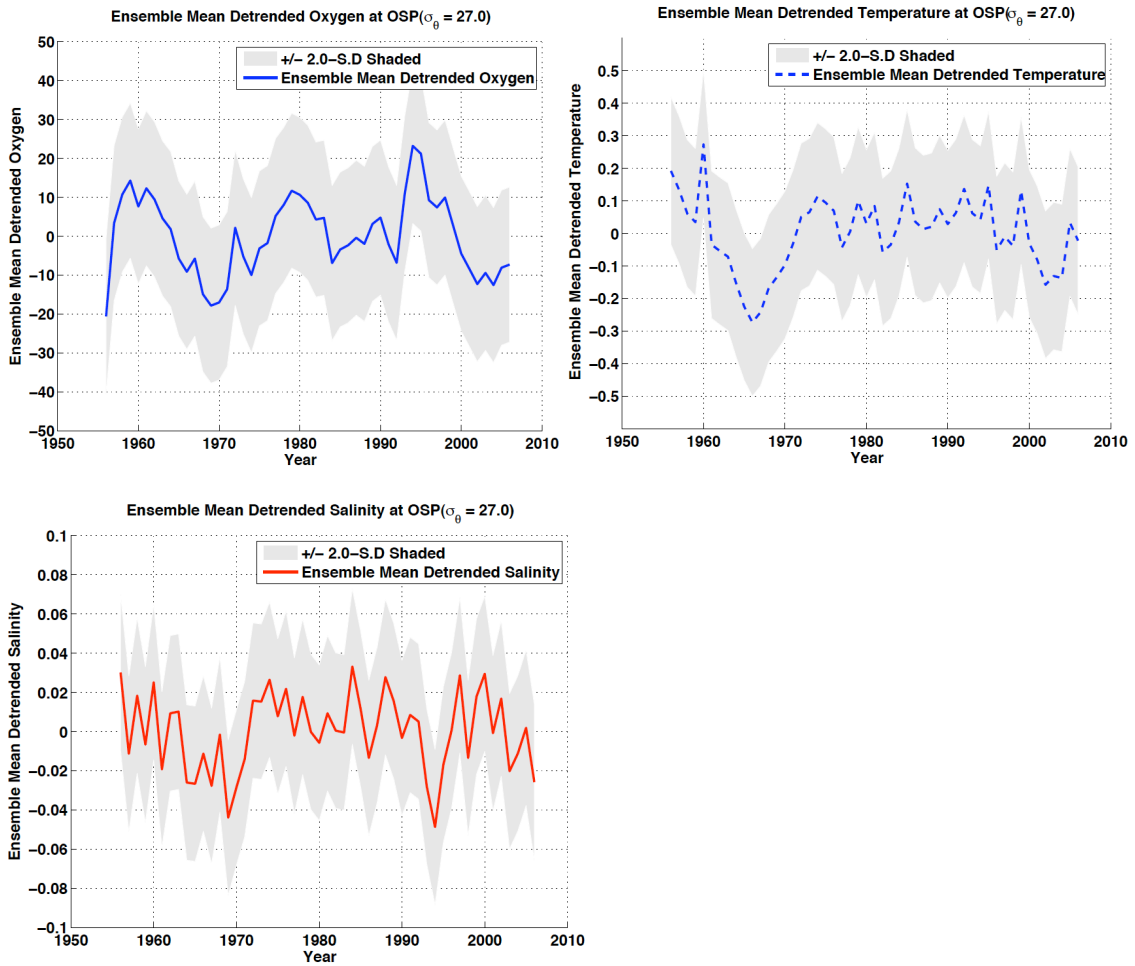


Figure 2-3. Detrended time series data based on the ensemble mean of the oxygen concentration, temperature, salinity and isopycnal depth at OSP from 1956 -2006 on the density surface $\sigma_\theta = 27.0$.

Standard deviation and lag-autocorrelation are essentially identical between annually binned data and ensemble mean data. Mean and standard deviation is calculated for the 51-year long time series as shown in Table 2-1. Standard deviation of temperature and salinity are small (approximately 4% of the mean temperature, 0.07% of the mean salinity) compared to oxygen concentration (approximately 20% of the mean oxygen). The oxygen variability is larger compared to temperature and salinity. Why is the oxygen

variability much more significant compared to temperature and salinity? This question is will be addressed later in chapter 3.

Lag-one autocorrelation coefficients and e-folding time scales for each variable are shown in table 2-2. Lag one auto-correlation coefficients are similar between oxygen and temperature (0.76 for oxygen, 0.79 for temperature). The oxygen and thermal anomalies are much more persistent than the salinity anomalies as shown by the e-folding time scales. The timescales are much shorter for salinity (1.3 year) compared to the oxygen and temperature (3.7 -4.3 years). These results indicate that oxygen and temperature have resemblance in lag-one autocorrelation and e-folding timescale. Even though the time scale between oxygen and temperature are similar, there is only small correlation between oxygen and temperature variability where cross-correlation coefficients is -0.07. However, the cross-correlation coefficient increases to 0.32 for the detrended time series.

Table 2-1

	Average (50 years)	S.D. (50 years)
Oxygen	57.3	11.04
Temperature	3.87	0.15
Salinity	33.99	0.023

51 years average and standard deviation (S.D.) of ensemble member time series for oxygen in units of $\mu\text{mol/kg}$, temperature in units of K and salinity in units of psu at OSP ($\sigma_{\theta} = 27.0$)

Table 2-2

	Lag 1 auto-correlation	e-folding timescale
Oxygen	0.76	3.7 year
Temperature	0.79	4.3 year
Salinity	0.46	1.3 year

Lag one auto-correlation and e-folding timescale calculated from lag auto-correlation. Auto-correlation and e-folding timescale are calculated from ensemble mean oxygen, temperature, salinity and isopycnal depth time series.

Ensemble members can provide additional information about the statistics of the time series at OSP. Figure 2-4 and 2-5 show the histograms of the mean, standard deviation and effective sample size for ensemble members for oxygen, temperature, salinity and isopycnal depth. The histogram of the mean and standard deviation in all the quantities are close to normal distribution. For oxygen concentration, peak of the histogram for mean and standard deviation are in the interval between 57-57.5 and 11.5-12.5. This is close to annual mean results in table 2-1. Similar features are seen in temperature, salinity and isopycnal depth (the interval of the mean and standard deviation peak are close to the annual mean results, see figures 2-4 and 2-5). The histogram of the effective sample sizes shows significantly different structure between oxygen/temperature and salinity. The effective sample size of the salinity is much larger than that of oxygen/temperature due to the lag-one autocorrelation (table 2-2). The skewness in the effective sample size in the salinity comes from the shorter de-correlation timescale which saturates at the record length of 50 years.

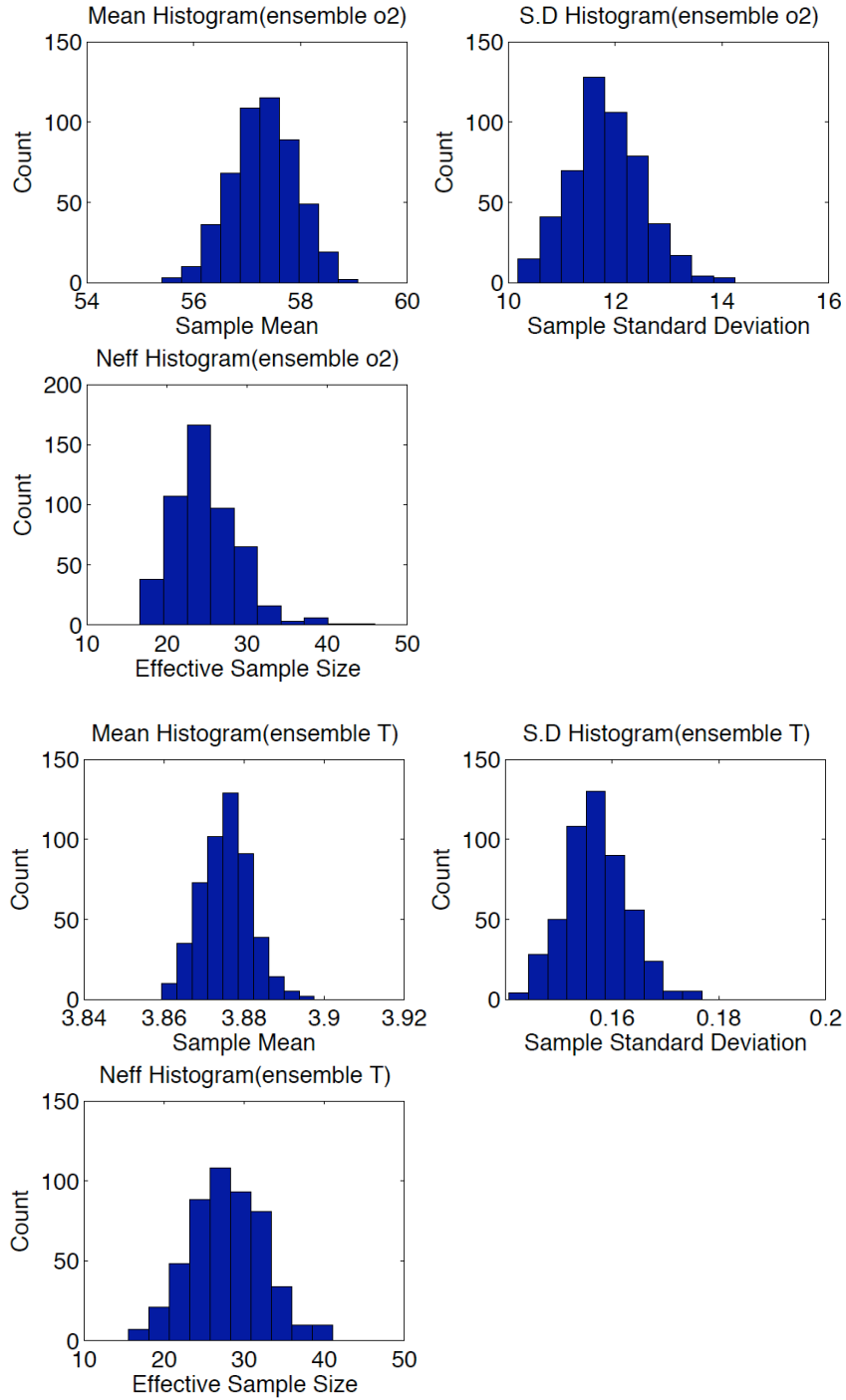


Figure 2-4. Histogram of mean, standard deviation and effective sample size calculated from 500 randomly sampled annual mean oxygen and temperature indices.

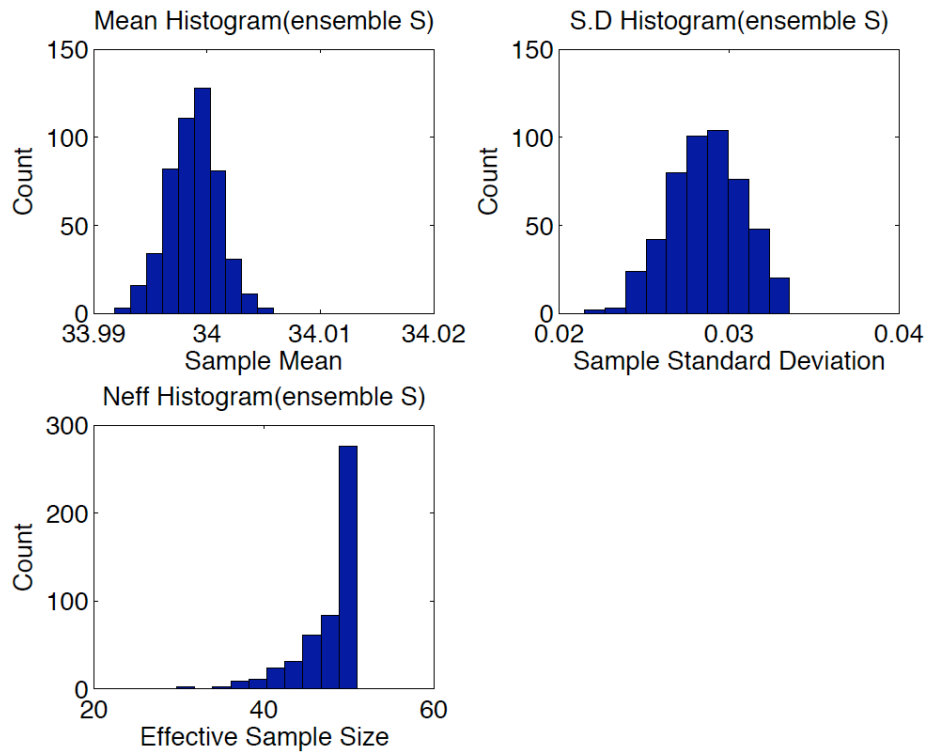


Figure 2-5. Same as in figure 2-4 except for salinity.

2-4. Results: Spectral Analysis

Figure 2-6 shows lag autocorrelation indices for ensemble mean time series data, indicating a unique structure in the oxygen data. Low-frequency variability of oxygen is revealed by a negative peak around 7-8 year lag and a positive peak in 16-17 year. This structure is absent in the temperature time series. While lag-one autocorrelation is similar between temperature and oxygen, the variability in the decadal timescale is significantly different between them.

Here we use two ways to compute the power spectrum of the time series. A periodogram can be constructed by calculating the Fourier transform of annually binned data as in Ito and Deutsch (2010). The algorithm used in spectral analysis is the discrete Fast Fourier Transform (FFT) routine in MATLAB.

Alternatively, ensemble of periodograms can be constructed by performing Fourier transform for individual ensemble members. This approach effectively removes the effect of averaging data with different sampling densities, and the resulting spectral density estimates have a simpler interpretation. Furthermore, the statistics of ensemble spectra can be used to test the robustness of the conclusions drawn from the previous study using the annually binned data.

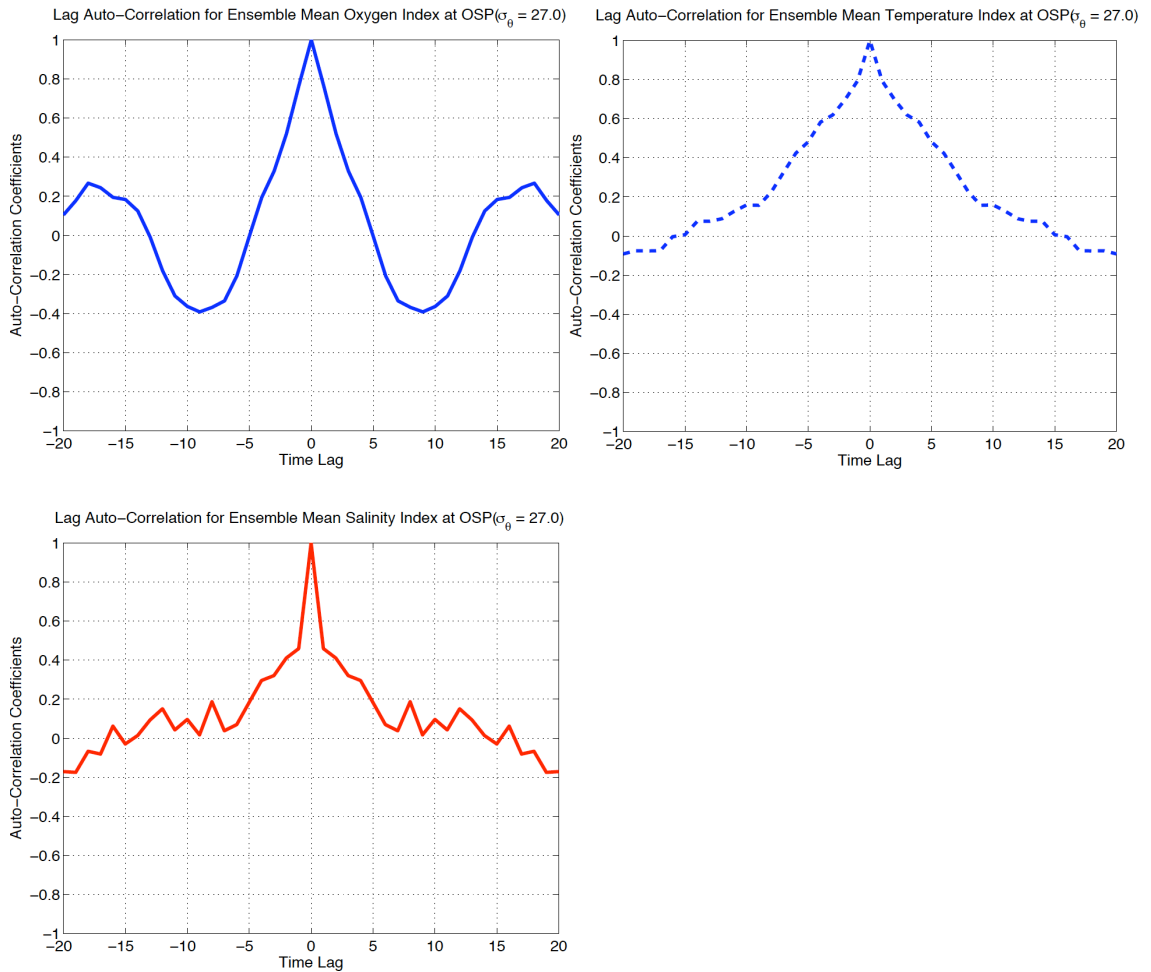


Figure 2-6. Lag-auto correlations for ensemble mean oxygen (blue solid), temperature (blue dash), salinity (red solid) and isopycnal depth (red dash). Ensemble means are calculated from simply taking an average of 500 ensemble members for each year.

First, the periodogram of annually binned data is shown in figure 2-7. The three panels show the periodograms of oxygen, temperature and salinity respectively. In the periodogram of oxygen, there is a significant spectral peak at 17^{-1} cycles/year. The statistical significance is tested with the 95% confidence interval determined from the theoretical red noise spectrum with one-tail test using F-distribution. This red noise spectrum represents the low-frequency variability explained by the integration of random

physical and biogeochemical variability by the slow, oceanic ventilation as discussed by Ito and Deutsch (2010). This stochastic model, in principle, applies to the variability of other passive tracers such as nutrients and carbon.

Similar peak is also found in temperature and salinity, however the peak is not statistically significant for temperature. The oxygen and temperature data contains significant low-frequency variability. Comparing the periodogram, there are resemblance in timescales between oxygen and temperature. 75% of the variance of oxygen is contained on the decadal and longer timescales. Similarly, 73% of the variance of temperature is contained on the decadal and longer timescales. The periodogram of salinity shows different features. There is a spectral peak at 2^{-1} cycles/year, and there is no statistically significant peak in the decadal timescale. In the frequency range higher than approximately 5^{-1} cycles/year, interannual variability contains 45% of salinity variance.

Spectral density is calculated for each ensemble member first. Then the average of spectral density estimates is determined as shown in figure 2-8. The two dash lines indicate the range containing 95% of ensemble members. Comparing figure 2-7 and 2-8, estimates of power spectra from both approaches show similar structures indicating low-frequency (decadal) variability of oxygen and temperature. Regarding the 15-20 year timescale variability of oxygen, almost all of the ensemble spectral density estimates exceed the 95% confidence interval of the theoretical red noise spectrum. This clearly demonstrates the robustness of low-frequency oxygen variability. Regardless of details in sampling, the observed oxygen time series data at OSP has increased power in the 15-20 year timescale. Furthermore, this ensemble approach brings additional information about

the oxygen spectrum. Focusing on the interannual timescales, some fraction of ensemble members exhibit statistically significant variability for the timescale of 5 years and shorter, and this also applies to the spectral density estimates of temperature and salinity. This indicates that depending on how data is sampled, interannual variability could also become significant in the OSP data.

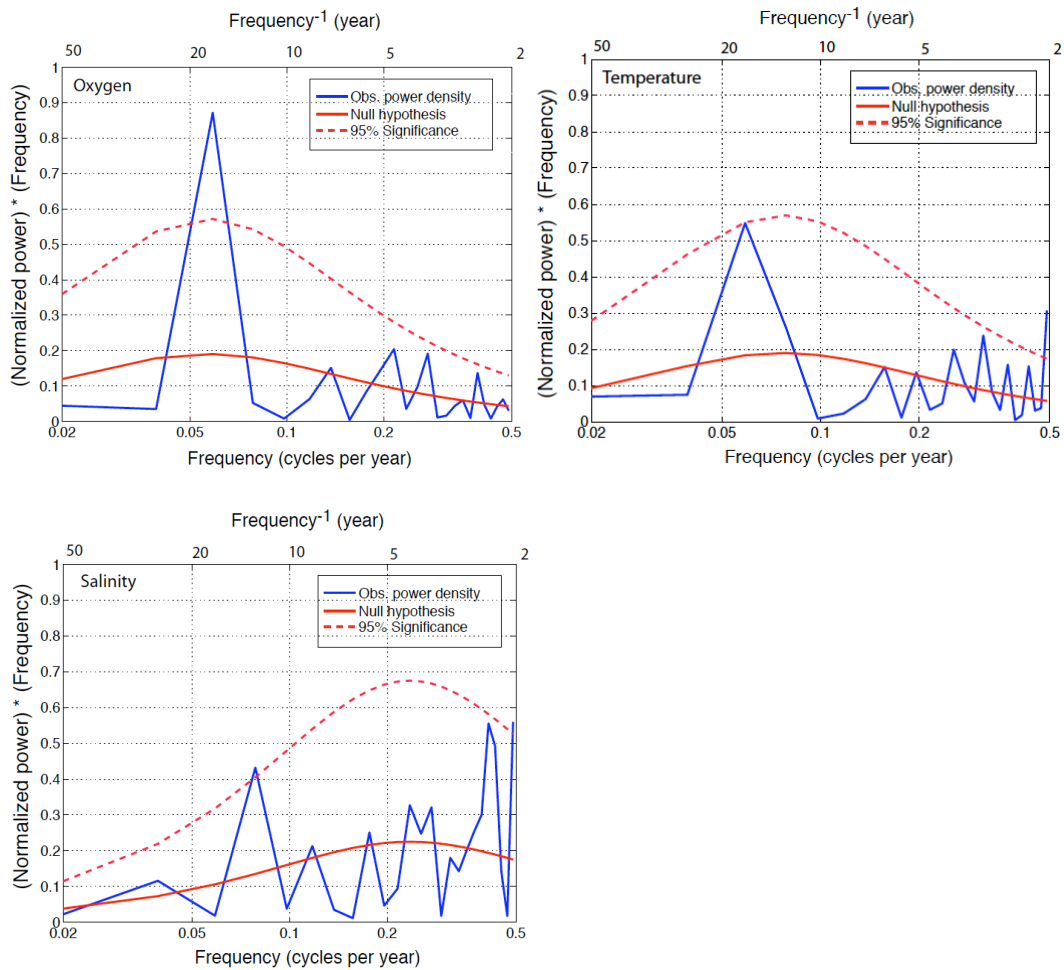


Figure 2-7. Power spectrum for annual mean observed data of oxygen, temperature and salinity in semi-log plot. Red lines are the red noise spectra calculated from the e-folding timescale and dashed black line shows the 95% significance threshold (based on a one-tailed test using the F-distribution).

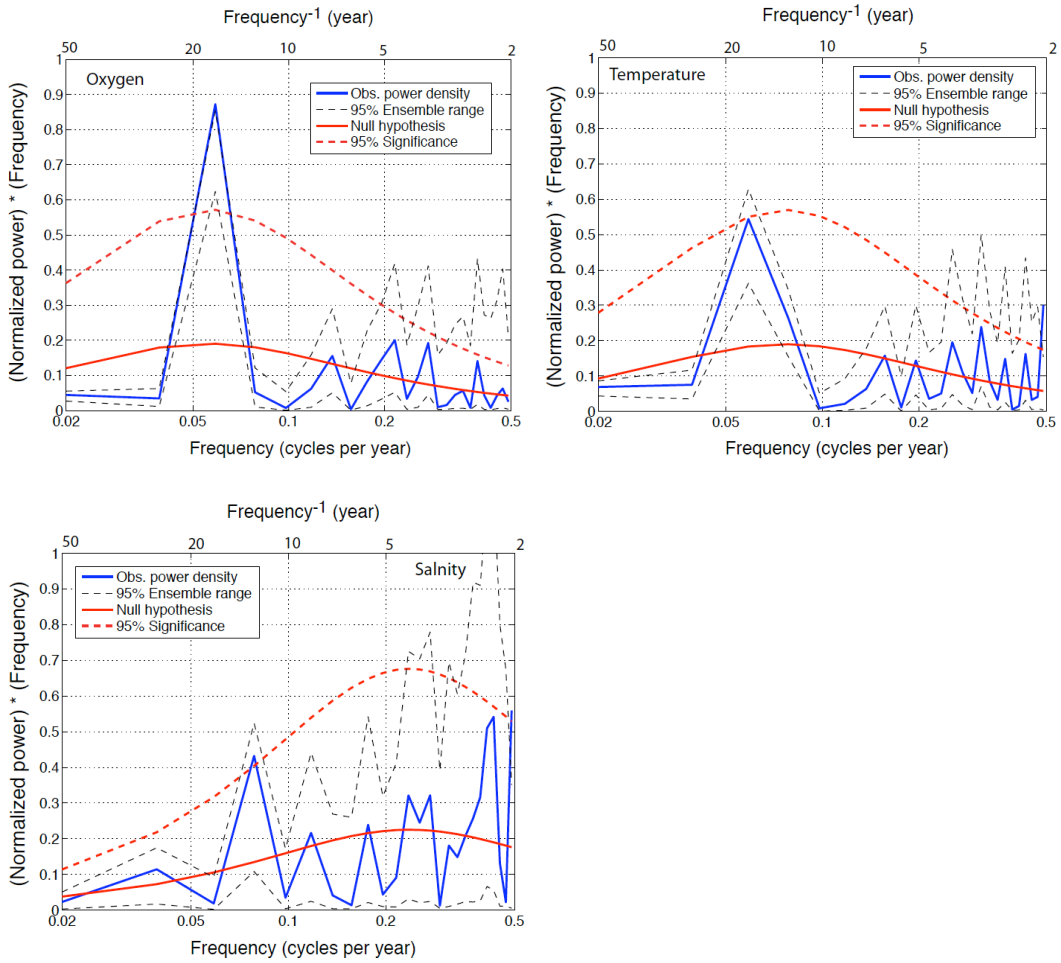


Figure 2-8. Power spectrum for ensemble mean observed data of oxygen, temperature, and salinity in semi-log plot. Red lines are the red noise spectra calculated from the e-folding timescale and dashed black line shows the 95% significance threshold (based on a one-tailed test using the F-distribution). Shading shows the range of the 95% of the ensemble member distribution.

2-5. Summary and Discussion

We analyzed the time series observation of temperature, salinity and oxygen on the density surface $\sigma_\theta=27.0$ at OSP motivated by the previous work of Ito and Deutsch (2010) where significant low-frequency variability is identified from the annually binned time series data. A new approach is introduced in this study where a subset of data is randomly sampled from the raw data to account for the varying sampling intervals in the original raw data. A robust statistics is developed based on the large number of ensemble members. In summary, we found:

- **A statistically significant spectral peak in the timescale of 15-20 years in almost all of the ensemble oxygen time series data**
- **Significant fraction of ensemble members also include statistically significant spectral peaks on the interannual timescales with periods shorter than 5 years**

Timescale inferred from the lag-one autocorrelation of oxygen data is similar to that of temperature and but not salinity. Salinity variability shows a stronger high-frequency variability (less than 5-years) indicating that there might be a separate mechanism driving the variability of salinity on the interannual timescales.

These new results indicate that the 15-20 year variability of dissolved oxygen in the Gulf of Alaska is robust, whose driving mechanisms are yet to be determined. Temperature and salinity data also show increased power density in this timescale,

however the spectral peak in temperature is not statistically significant at 95% confidence interval. Because the temperature and salinity also show increased low-frequency variability there could be a common mechanism driving the variability of oxygen, temperature and salinity. Furthermore, there are smaller but potentially significant variability on the interannual timescales, which was not detected in the previous studies using annually binned data.

We have not yet examined the statistics over the seasonal timescale due to the sparse sampling density after 1980s. It may be possible to separate the data into warm and cold seasons and conduct statistical analysis to examine the role of seasonality, which is left for future study. Extracting low-frequency and high-frequency component of the time series using some filtering method may also be another approach to see the detailed features of low and high frequency variability.

These results motivate further investigation to better understand mechanisms driving the variability of dissolved oxygen in the subpolar North Pacific. What are the causes of the strong variability on the 15-20 year timescale? What are the link between oxygen and physical parameters such as salinity and temperature? So far, our investigation focused on the analysis of existing observational data. It is difficult to address these questions based on observational data analysis alone, and in the next chapter, a new modeling approach is developed to formulate and to test hypotheses for the causes of the observed oxygen variability.

CHAPTER 3. MODELING THE LOW FREQUENCY VARIABILITY OF OXYGEN IN THE NORTH PACIFIC

3-1. Background

In the previous chapter, we identified a robust low-frequency variability on the timescale of 15-20 years in the observed thermocline oxygen time-series data at Ocean Station Papa (OSP). What controls the low-frequency variability of the thermocline oxygen in the subpolar North Pacific? It is known that the low-frequency variability of oxygen is also found in the western Pacific (Ono et al., 2001). Furthermore there is a known anti-correlation of thermocline oxygen between the eastern and western subpolar North Pacific (Watanabe et al., 2008). These previous results indicate the potential role of large-scale climate processes in controlling the variability of biogeochemical tracers in the entire subpolar North Pacific region. Ito and Deutsch (2010) also noted a significant correlation between the thermocline oxygen at OSP and the North Pacific Gyre Oscillation index (Di Lorenzo et al., 2008) between 1980 and 2007 (correlation coefficient is 0.64, 95% confidence interval). While there are accumulating evidences for the existence of the large-scale, low frequency variability of oxygen in the North Pacific, the mechanisms driving this variability is poorly understood. In this chapter, we will use the combination of statistical analysis and numerical modeling to better understand the

primary factor controlling this variability and to offer a consistent interpretation of previous observations.

In section 3-2, we first investigate the empirical relationship between oxygen variability at OSP and ocean circulation fields over the North Pacific, revealing a large-scale pattern of barotropic stream function associated with the thermocline oxygen anomaly at OSP. In section 3-3, we will present a hypothesis based on the results from the statistical analysis, suggesting the characteristics of the ocean circulation fields that are connected to the oxygen variability. In section 3-4, we describe a new numerical model of transport-driven oxygen anomaly, which is used as a tool to test the hypothesis. The model captures many aspects of the observed oxygen variability at OSP. In section 3-5, we perform empirical orthogonal function (EOF) analysis of the simulated oxygen field, revealing the link between the basin-scale oxygen variability and the modes of climate variability in the North Pacific. In section 3-6, we summarize and discuss the implication of our results.

3-2. North Pacific Circulation and Thermocline Oxygen

Physical circulation fields from the Estimating the Climate and Circulation of the Oceans (ECCO) project are extensively used in this study. The ECCO project is an international effort to constrain three dimensional physical ocean circulation fields using a suite of in-situ and remotely sensed oceanic observations including temperature (T) and salinity (S) from historic hydrographic measurements and buoys, satellite sea surface temperature, sea surface height and T and S from autonomous floats. The specific dataset

used in this study comes from the German part of the ECCO effort (GECCO) to estimate the ocean circulation over the period 1952-2001 paralleling the 50-year NCEP/NCAR reanalysis. We use the monthly-mean ocean circulation fields from the GECCO dataset (Köhl, et al, 2007) where the Massachusetts Institute of Technology ocean general circulation model (MITgcm; Marshall et al., 1997a, b) is brought into consistency with observations using the adjoint method (Marotzke et al., 1999; Wunsch and Heimbach 2007). The estimation effort covers the 50-year period from 1952 January through 2001 December, and the detailed procedures of data assimilation are documented in Köhl et al., (2007). We have used the GECCO dataset including potential temperature, salinity, and zonal (u) and meridional velocity (v) fields.

First, using the monthly mean velocity field, we calculated the barotropic streamfunction. We first vertically integrated the zonal velocity as follows.

$$U = \int_{-H}^0 u dz \quad (3-1)$$

where $-H$ is the depth of the bottom topography. Then we meridionally integrated the vertically integrated zonal velocity (U) from north to south as follows.

$$\Psi = \int_y^{y_2} U dy \quad (3-2)$$

where y_2 is the latitude of the northern topographic boundary of the North Pacific basin and y is the arbitrary latitude. The topography of the model does not include the open channel at the Bering Strait, so there is no mass exchange between the Pacific and Arctic Ocean. While the equation (3-2) is written in Cartesian coordinate, the actual calculation

was performed in the spherical coordinate. The resulting $\Psi(x,y,t)$ is the monthly barotropic streamfunction field in units of volume flux, m^3/s .

We statistically analyzed the monthly mean barotropic stream function to find relationships between the observed oxygen variability at OSP and the ocean circulation over the North Pacific. The statistical significance of the correlation coefficients field is estimated by testing whether the correlation coefficients are significantly different from zero based on t-test. Linear correlation and regression analysis are based on winter mean (December-January-February mean: hereafter DJF mean) barotropic stream function since the atmospheric variability over the North Pacific is the strongest in winter.

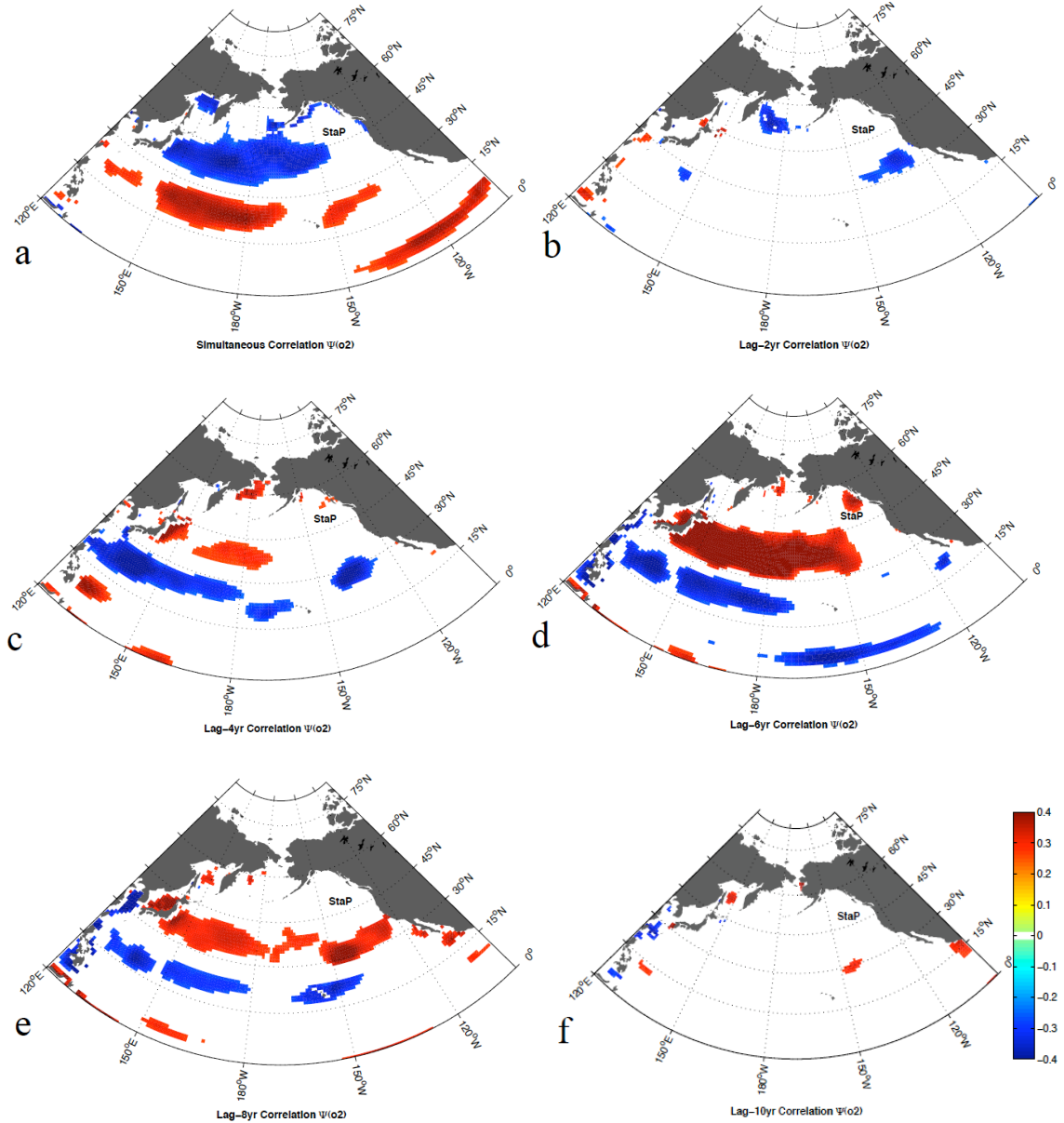


Figure 3-1. Lag-correlation coefficients between dissolved oxygen time series at OSP ($\sigma_{\theta} = 27.0$) and the DJF mean barotropic stream function over the North Pacific. (a-f) Simultaneous to lag 10-year correlation maps are shown. Red shading shows the positive correlation coefficients and the blue shading shows the negative correlation coefficients respectively. Areas exceeding significance levels of 95% based on t-test are shaded. The StaP in the figure is the approximate location of OSP.

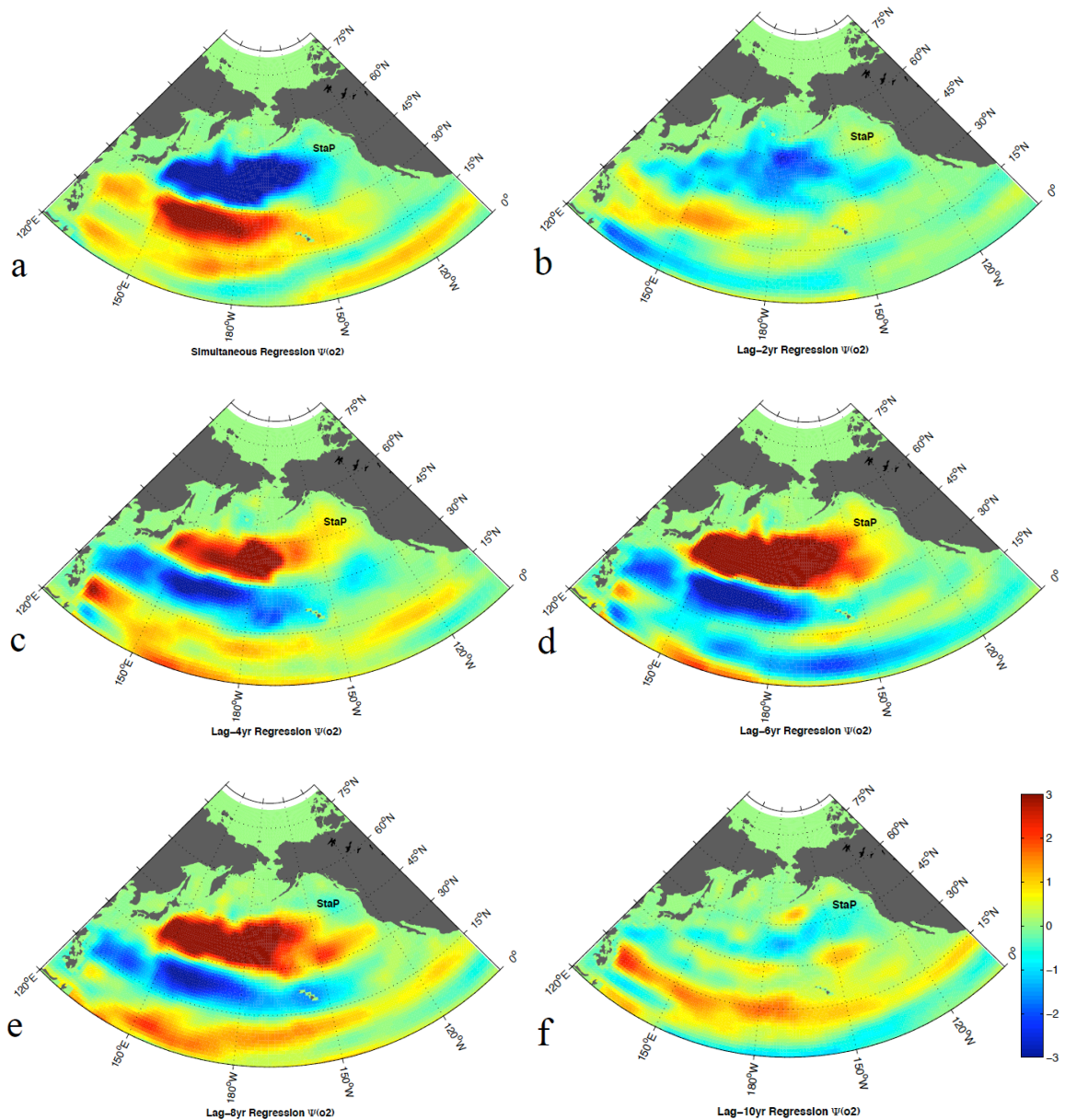


Figure 3-2. Lag-regression coefficients between dissolved oxygen time series at OSP ($\sigma_\theta = 27.0$) and the DJF mean barotropic streamfunction over the North Pacific. (a-f) Simultaneous to lag 10-year regression maps are shown. Red shading shows the positive regression coefficients and the blue shading shows the negative regression coefficients respectively. Units are in Sverdrup [Sv].

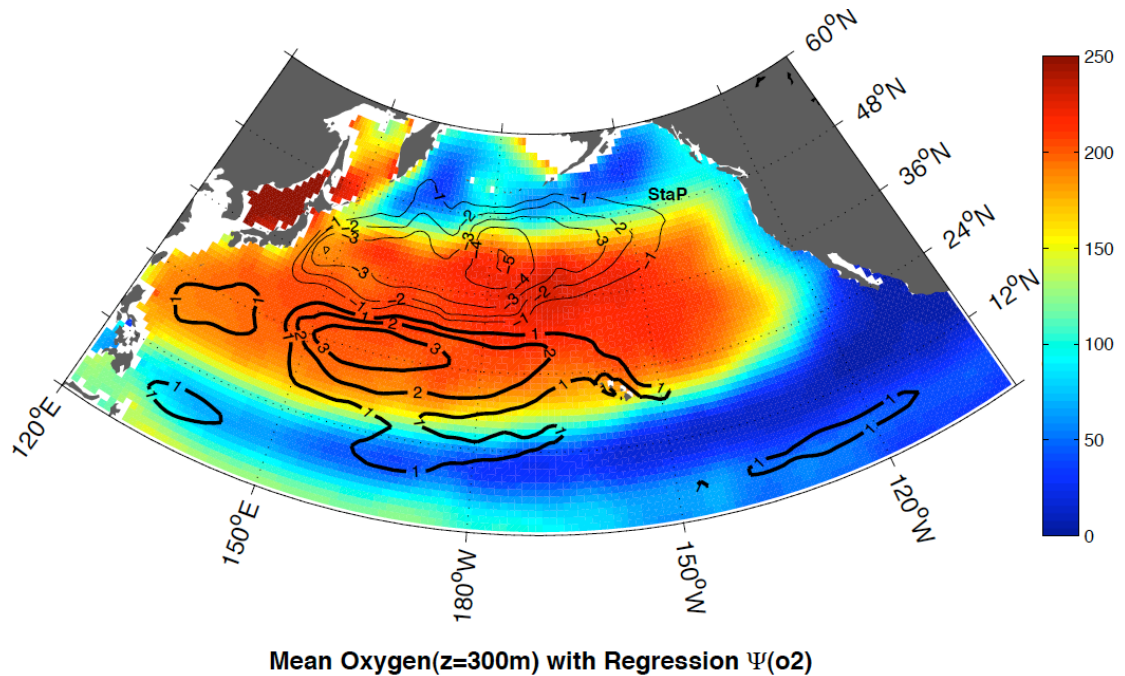


Figure 3-3. Climatological oxygen distribution in the thermocline (300m depth) over the North Pacific, and simultaneous regression coefficients between dissolved oxygen time and barotropic streamfunction (in contour (positive values in thick line), same as in figure 3-2a). Barotropic streamfunction is in the units of Sv ($10^6 \text{ m}^3/\text{s}$). The StaP in the figure is the location of OSP.

Figure 3-1 and 3-2 show the simultaneous and lag correlation and regression coefficients between observed annual mean oxygen index at OSP ($\sigma_\theta = 27.0$) and the DJF mean barotropic stream function. First, we focus on the simultaneous correlation and regression (figure 3-1a and 3-2a). The correlation and regression coefficients show a north-south dipole pattern including a negative anomaly in the Kuroshio extension region and positive anomaly at the south of this region. The negative value in the north corresponds to a cyclonic circulation, and the positive value in the south is an anti-cyclonic circulation. Thus, this pattern indicates the intensification of eastward flow at about 30°N and associated spin-up of the double gyres, positively correlated with the

thermocline oxygen at OSP.

Furthermore, lag-correlation/regression coefficients indicate that this pattern is persistent for about a year before it decays away. With the lag (oxygen lagging behind the barotropic stream function) of between 5 and 8 years, the sign of the dipole pattern reverses. The sign reversal of the dipole pattern and associated spin-down of the double gyre could be the key to understand the quasi-periodic behavior of the thermocline oxygen over the decadal timescales. The dipole pattern of the correlation and regression coefficients has a direct implication for the generation of oxygen anomaly in the subpolar North Pacific. Figure 3-3 shows the background, climatological distribution of oxygen in color shading based on the World Ocean Atlas 2005 (Garcia et al., 2006). The well-ventilated, subtropical thermocline is well oxygenated due to the subduction (downward transport) of surface waters by the mean gyre circulation. In contrast, the upwelling regions of subpolar and tropical North Pacific are depleted in oxygen due to the lack of oxygen supply from the surface. Thus there is a strong north-south gradient in the mean oxygen concentration at the subtropical-subpolar boundary at approximately at 45°N.

The dipole pattern of barotropic stream function (taken from the regression coefficients plotted in figure 3-2) is superimposed as contour lines over the background mean oxygen distribution in figure 3-3. While the barotropic stream function reflects the vertically integrated volume transport, much of the transport occurs in the upper ocean. The cross-gradient advection of mean oxygen is clearly depicted in figure 3-3. The northern, cyclonic cell of the double gyres drives the northward advection of high-O₂ water into the eastern subpolar North Pacific and the southward advection of low-O₂ water into the western subpolar North Pacific. Thus, the advective transport of

background mean oxygen driven by this basin-scale, subpolar circulation can explain the higher oxygen concentration at OSP and the lower oxygen in the western North Pacific by modulating the subtropical-subpolar boundary as marked by the strong north-south gradient of the mean oxygen concentration.

The sign reversal of the dipole pattern over the 5-8 year timescale can explain the oscillatory behavior of the zonal dipole of oxygen in the subpolar thermocline. When the subpolar circulation reverses its sign, the advection of mean oxygen also reverses its sign. This leads to a negative tendency of anomalous oxygen in the east and a positive tendency in the west. The anticipated anomalies are anti-correlated between the eastern and western North Pacific consistent with the previous observations. This mechanism can potentially explain the quasi-periodic behavior of the thermocline oxygen at OSP where the sign reversal of the double gyre pattern in every 5-8 years can translate into the alternating oxygen anomalies on the decadal timescales.

3-3. Hypothesis

Empirical relationship between observed thermocline oxygen anomalies and the vertically integrated ocean circulation fields imply an important role of basin-scale circulation variability driving the low-frequency variability of oxygen in the North Pacific. Here is the summary of the empirical analyses so far.

- **The north-south dipole pattern of barotropic stream function is significantly correlated with the thermocline oxygen at OSP.**

- **The northern cell of the dipole crosses the strong north-south gradient of background mean oxygen.**
- **The dipole pattern reverses sign over the timescale of 5-8 years.**

Thermocline oxygen at OSP is most strongly influenced by the northern cell due to its location. The advection by the northern cell crosses the background mean gradient of oxygen at the subtropical-subpolar boundary, which can generate the observed east-west anti-correlation of thermocline oxygen anomalies identified in the previous studies (Watanabe et al., 2008). The reversal of the dipole pattern can potentially force the reversal of the oxygen anomalies on the 5-8 year timescales, leading to the quasi-periodic oxygen variability on the timescales overlapping the observed spectral peak of the thermocline oxygen at OSP.

We hypothesize that the low-frequency variability of thermocline oxygen in the subpolar North Pacific is primarily caused by the large-scale circulation variability acting on the strong subtropical-subpolar gradient of mean oxygen concentration. Due to the configuration of mean oxygen gradient, the circulation variability is likely to generate opposite-sign oxygen anomalies between the eastern and western subpolar North Pacific.

To test the above hypothesis, we construct a three-dimensional numerical model of oxygen anomaly driven by the data-constrained circulation fields from the GECCO dataset. In the calculation, the effect of air-sea gas exchange and biological variability is suppressed such that the simulated oxygen anomaly is solely driven by the circulation variability. The simulated oxygen anomalies are tested against the observed thermocline oxygen at OSP, and the spatial-temporal variability will be analyzed in detail.

3-4. A Three-dimensional Simulation of Oxygen Anomaly

Three-dimensional distribution of oxygen anomaly is simulated using the MITgcm in the global ocean configuration with the lateral resolution of $1^\circ \times 1^\circ$ in longitude-latitude grid and the 23 vertical layers. The pre-determined circulation fields are used to advect the oxygen anomaly as a passive tracer. First, the linearized tracer continuity equation for oxygen anomaly can be written as follows.

$$\frac{\partial O'_2}{\partial t} + \bar{\mathbf{u}} \cdot \nabla O'_2 - \nabla \cdot \mathbf{K} \nabla O'_2 = -\mathbf{u}' \cdot \nabla \bar{O}_2 \quad (3-3)$$

where the diffusion tensor \mathbf{K} includes the parameterization of sub-grid scale eddies following Gent and McWilliams (1990), KPP mixed layer scheme (Large et al., 1994) and a small background turbulent diffusion with the vertical diffusivity of $10^{-5} \text{ m}^2/\text{s}$. The oxygen anomaly is transported by the time-mean circulation as determined by the long-term mean circulation fields of the GECCO product. On the RHS of the equation (3-3) there is a source term of oxygen anomaly driven by the anomalous circulation transporting the climatological mean oxygen concentration as determined by the World Ocean Atlas 2005 (Garcia et al., 2006). In this model, air-sea gas exchange process and biology effects are turned off so it is purely driven by the physical transport, and the boundary condition at the surface is $O_2' = 0$.

Initializing with the globally uniform oxygen anomaly of zero, we integrate the oxygen anomaly model from 1952 January through 2001 December, and the monthly mean oxygen anomaly fields are archived for the simulation period. The model generates

the three-dimensional, global distribution of transport-driven oxygen anomaly, and this study focuses on the North Pacific region.

Figure 3-4 shows the detrended oxygen anomaly from the observation and the model at the location of OSP on isopycnal layer ($\sigma_{\theta} = 27.0$). Model captures many aspect of the observed oxygen at OSP. The correlation coefficient between observed and modeled oxygen anomaly at OSP is 0.75 (significant at the 95% level). Figure 3-5 shows the standard deviation of modeled oxygen on two isopycnal layers ($\sigma_{\theta} = 26.5$ and 27.0). The Gulf of Alaska shows an elevated standard deviation in both isopycnal layers. The magnitude of standard deviation field is higher on shallower layer, and it also shows a strongly variability in the subpolar Pacific relative to the subtropics.

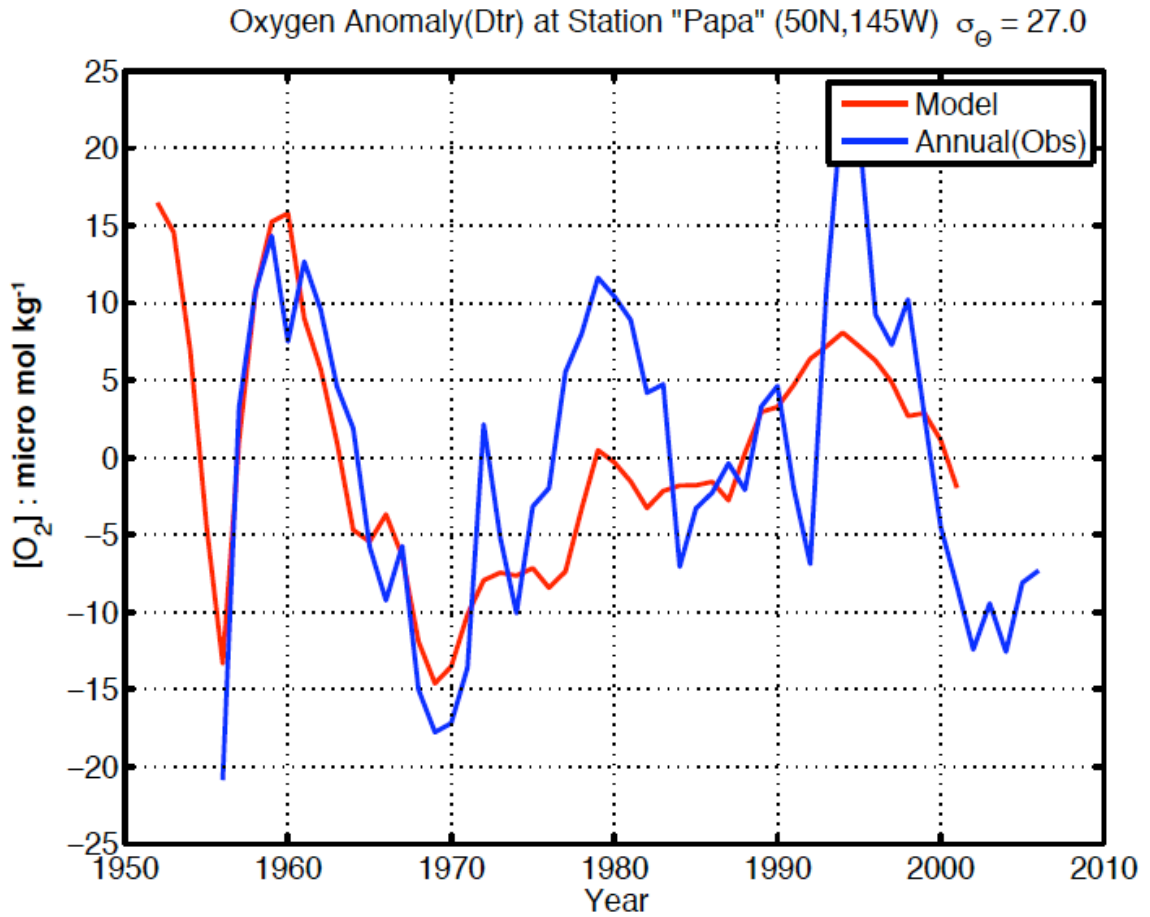


Figure 3-4. Dissolved oxygen anomaly at OSP (on isopycnal layer, $\sigma_{\theta} = 27.0$) from observational data and model output data. Observational oxygen is anomaly from the climatology. Both indices are detrended.

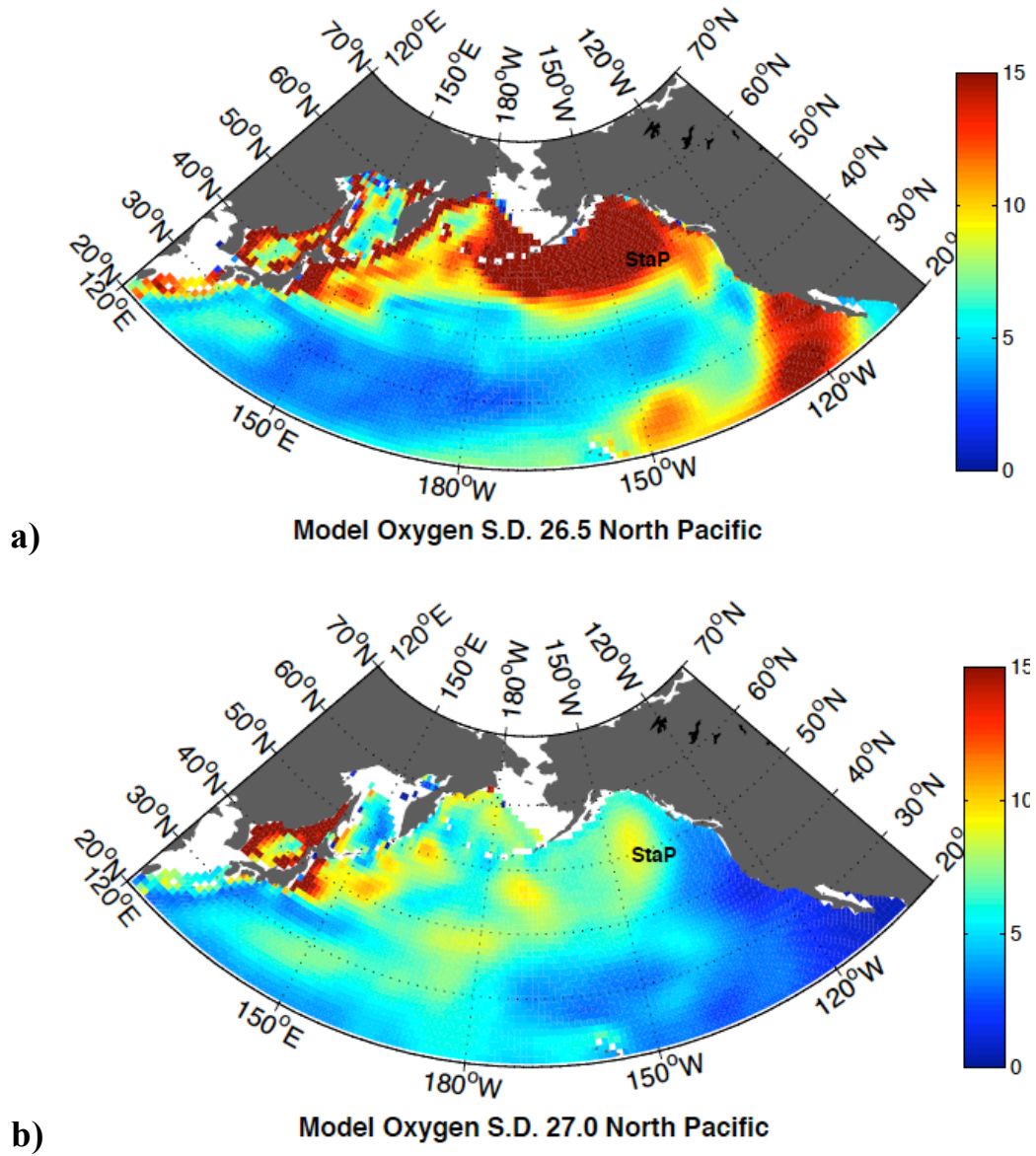


Figure 3-5. Standard deviation of oxygen anomaly field on two isopycnal layer, (a) $\sigma_\theta = 26.0$, (b) $\sigma_\theta = 27.0$ from model output.

3-5. Climate-driven Oxygen Anomaly

To investigate the dominant pattern of the transport-driven oxygen anomaly on isopycnal layer ($\sigma_{\theta} = 27.0$), we conducted an Empirical Orthogonal Function (EOF) analysis on the simulated thermocline oxygen anomaly over the North Pacific (the domain is 20°N-70°N, 120°E-100°W). The EOF analysis is applied to the deseasonalized model output weighted by the square root of the cosine of latitude. Figure 3-6 shows the first and second EOF spatial pattern (correlation coefficients between principal component (PC) time series and model oxygen anomaly, upper panels) and the PC time series (lower panels). The first EOF pattern shows a strong positive oxygen anomaly from western subtropical Pacific extending into the Gulf of Alaska region, and both the first and second EOF show a strong east-west dipole pattern (opposite phase between the Gulf of Alaska and the western subpolar region). The explained variances of first and second EOF are 33% and 17.9% respectively. This spatial pattern indicates that the both first and second EOFs are important explaining the oxygen variability over the Gulf of Alaska including the location of the OSP. Temporal variability of the first EOF (PC1 time series) shows positive trend from 1950s to 2000s. Both PC1 and PC2 time series show low-frequency variability but a stronger decadal variability is found in the PC2 time series. There is a major phase shift in PC2 before and after 1970s. This shift might be related to the climate shift in 1970s as we discuss below.

To better understand the relationship between the climate variability and the dominant modes of the thermocline oxygen, we conducted an EOF analysis on the sea surface temperature (SST) from the GECCO data. Figure 3-7 shows the same EOF

pattern and PC time series as in figure 3-6 except for SST. PC time series in figure 3-7 (lower panels) are superimposed with the oxygen PC time series. Spatial pattern of the first EOF of SST shows a PDO-like pattern, and the second EOF of SST shows a pattern that is related to the North Pacific Oscillation (NPO) (Linkin and Nigam, 2008). The explained variances of first and second EOF of SST are 20.9% and 9.3% respectively. Comparing the results from EOF analysis on model oxygen and SST, the first EOF of oxygen anomaly is strongly correlated with the second EOF of SST (correlation coefficient is 0.72) and the second EOF of oxygen anomaly is strongly correlated with the first EOF of SST (correlation coefficient is 0.5). These results indicate that the dominant pattern of thermocline oxygen variability can be well explained by the leading modes of SST.

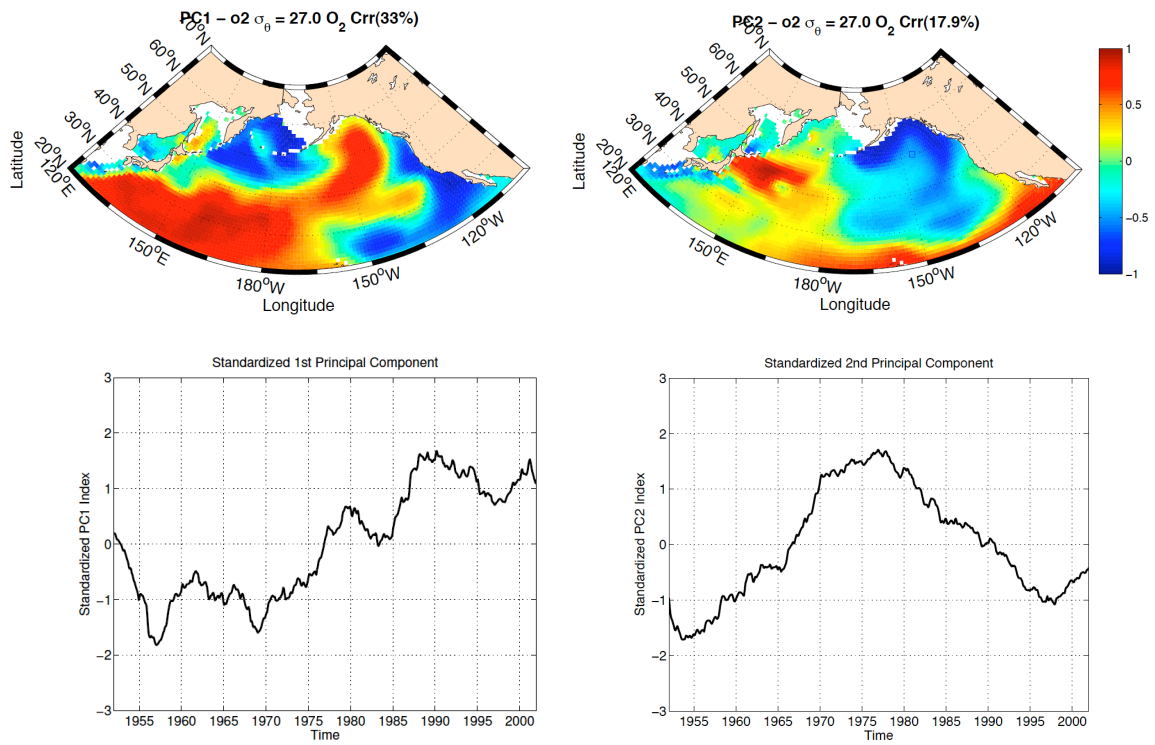


Figure 3-6. The first and second EOF spatial pattern and principal component based on model oxygen anomaly from 1952 - 2001. The spatial patterns are the correlation coefficients between principal component indices and model oxygen anomaly fields. The principal component indices are standardized by mean and standard deviation.

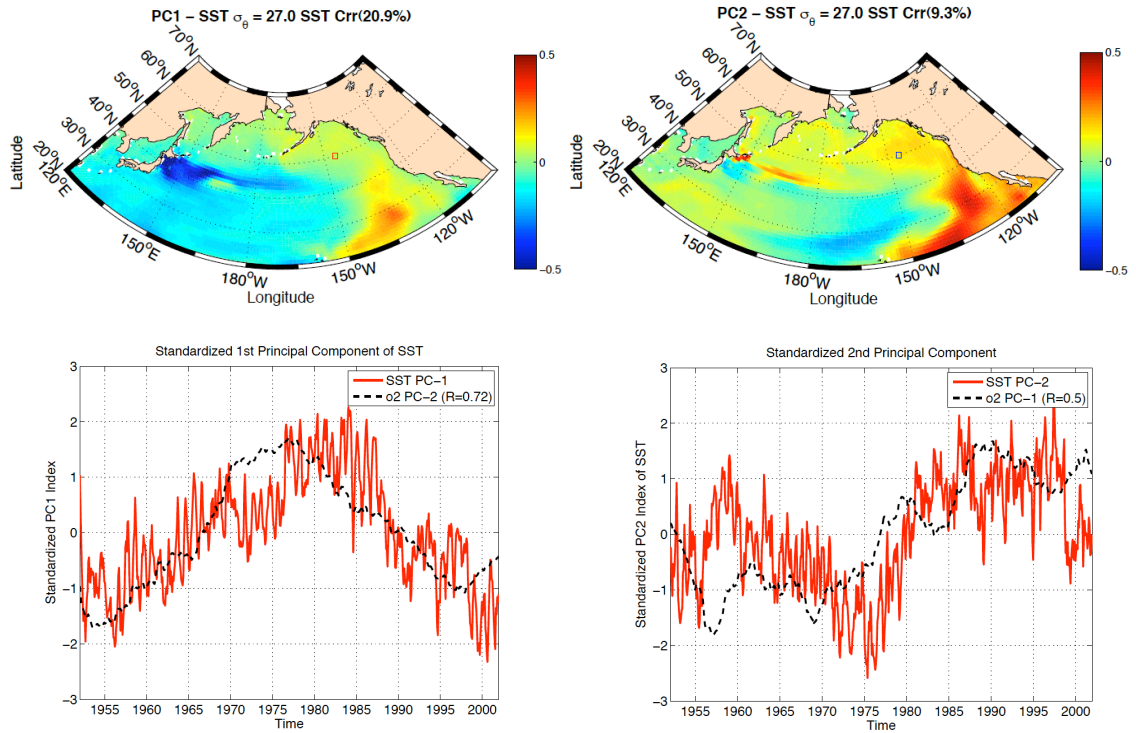


Figure 3-7. The first and second EOF spatial pattern and principal component based on GECCO sea surface temperature from 1952 - 2001. The spatial patterns are the correlation coefficients between principal component indices and GECCO sea surface temperature. The principal component indices of SST and corresponding oxygen modes are plotted in the lower panels. The principal component indices are standardized by mean and standard deviation.

Based on the model anomaly fields, we diagnosed the transport divergence of oxygen anomaly for the region around the OSP (defined as a box bounded by 140°W-150°W, 45°N-55°N, 223m-610m depth) evaluating the dominant component of oxygen tendency (horizontal or vertical advection). Figure 3-8 shows two panels for the time series of oxygen transport divergence in the Gulf of Alaska including (top) the advection of mean oxygen by the anomalous circulation and (bottom) the advection of anomalous oxygen by the mean circulation. The transport divergence driven by the anomalous circulation (Figure 3-8a) contains more high frequency variability compared to that driven by the mean circulation (Figure 3-8b). Then the transport divergence is separated into the zonal, meridional and vertical components, showing that horizontal transport is the dominant driver of the transport divergence. For the mean advection, the magnitudes of meridional and vertical components are significantly smaller compared to the zonal component. These results show an important role of lateral advection: zonal component is dominant for the transport of anomalous oxygen by the mean flow (correlation coefficient between transport of anomalous oxygen and zonal transport is 0.98), and the meridional component is dominant for the transport of background-mean oxygen by the anomalous flow (correlation coefficient between transport of mean oxygen and meridional transport is 0.6).

These results are in consistency with our hypothesis that the horizontal circulation variability is the primary driver of the oxygen variability in the subpolar North Pacific. For the location of the OSP, both the advection of mean oxygen and anomalous oxygen are both important in controlling the time-evolution of the oxygen in the region.

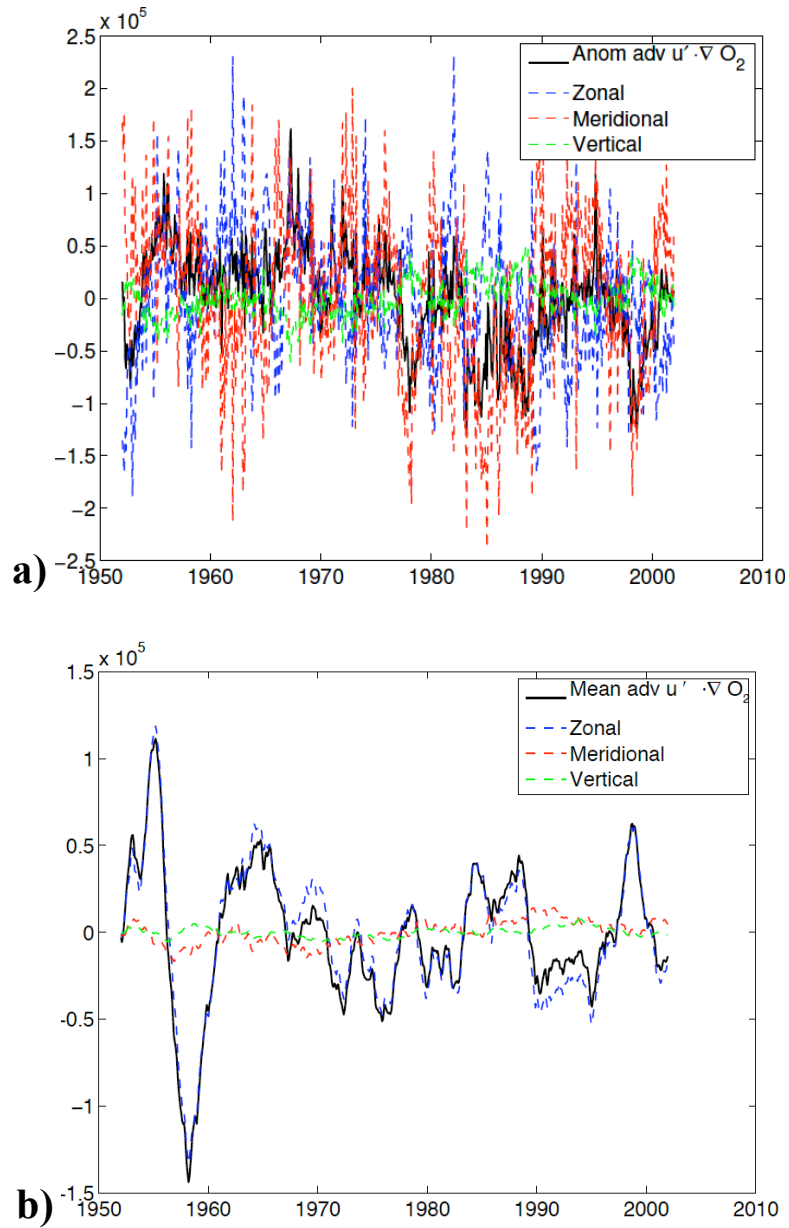


Figure 3-8. Oxygen transport budget over the Gulf of Alaska (box-region 140W-150W, 45N-55N, 223m-610m depth). Figure 8a shows the transport budget for mean oxygen driven by anomalous current and 8b shows the transport budget for anomalous oxygen driven by mean circulation.

3-6. Summary and Discussion

Motivated by the significant correlation between the thermocline oxygen at OSP and the basin-scale barotropic stream function, we performed a three-dimensional numerical simulation of the transport-driven oxygen variability for the period of 1952 to 2001. We found that the significant fraction of observed oxygen variability (correlation coefficient is 0.75, 95% confidence interval) over the Gulf of Alaska is captured by the model. Here are the summaries of the key results.

- **More than 50% of variance of thermocline oxygen is explained by the first two EOF in the extratropical North Pacific.**
- **The first PC of thermocline oxygen is significantly correlated with the second PC of SST ($R=0.7$) associated with the North Pacific Oscillation.**
- **The second PC of thermocline oxygen is significantly correlated with the first PC of SST ($R=0.5$) associated with the Pacific Decadal Oscillation**
- **Diagnosis of oxygen transport divergence indicate the important role of horizontal advection**

The circulation pattern associated with oxygen variability involves the north-south dipole pattern in the barotropic streamfunction. The EOF analysis of the simulated oxygen anomaly shows that the dominant mode of the oxygen anomaly over the North Pacific can be well explained by the basin-scale SST variability (PDO and NPO). The PCs of SST includes significant high-frequency component which is missing in the

thermocline oxygen because the relatively slow circulation of the thermocline waters tend to average out the effect of rapidly varying fluctuations relative to the ventilation timescale of the thermocline waters (Ito and Deutsch, 2010), making a natural low-pass filter of the climate signals in the oceans.

While the model can capture overall structure of the oceanic oxygen variability in the North Pacific, there are several limitations in this model. First, the model intentionally removes the effect of air-sea gas exchange and biological variability, which can be an important driver of oxygen variability in certain regions. Thus our estimates of oxygen variability may deviate from the true variability in some regions. These limitations can be overcome by including the representation of air-sea gas exchange and biology, which is left for the future study. Secondly, there could be errors in the circulation fields used in this study, which can introduce errors in our estimates of the oxygen anomalies. Even though the data-constrained physical circulation fields from the GECCO project is among the best estimates of the state of the oceans, oceanographic observations are sparse especially before the satellite era.

This study identified links between the thermocline oxygen and the modes of surface climate variability such as the NPO and PDO modes and the crucial role of the lateral transport. The ultimate cause of the low-frequency variability of thermocline oxygen is dependent on the behavior of the physical climate variability including the coupled ocean-atmosphere climate variability and its impact on the marine biogeochemistry.

CHAPTER 4. CONCLUSIONS

This study aims to better understand the variability of thermocline oxygen in the subpolar North Pacific. We first analyzed the observed thermocline oxygen in the Gulf of Alaska where the longest time series data is available in this region. We examined the robustness of its low-frequency variability, and then investigated the mechanism controlling this low-frequency variability.

We performed an improved time series analyses without making excessive averaging of the raw data by randomly sub-sampling the data and generated ensemble time series. Even though the data is irregular in sampling frequency, and the 50-year long record length can only capture several cycles of decadal fluctuations, we were able to test the robustness of the low-frequency variability. A statistically significant spectral peak in the timescale of 15-20 years is found in almost all of ensemble members, and significant fraction of ensemble members also include statistically significant spectral peaks on the interannual timescale with periods shorter than 5 years. Spectral analysis shows similar timescale between dissolved oxygen and temperature but however, these two are not strongly related.

We investigated the causes of the strong variability on the 15-20 year timescale and the link between oxygen and physical circulation fields. There is a statistically significant relationship between observed oxygen at OSP and the barotropic stream function of the North Pacific basin based on the GECCO data. The north-south dipole

pattern of barotropic stream function is significantly correlated with the thermocline oxygen at OSP and the northern cell of the dipole crosses the strong north-south gradient of background mean oxygen. This dipole pattern reverses sign with the lag timescale of 5-8 years. Thermocline oxygen at OSP is most strongly influenced by the northern cell due to its location. The advection by the northern cell crosses the background mean gradient of oxygen at the subtropical-subpolar boundary, which can generate the observed east-west anti-correlation of thermocline oxygen anomalies identified in the previous studies. Based on these analyses, we hypothesize that physical circulation variability acting on the background mean oxygen gradient could be the key in controlling the low frequency in the dissolved oxygen.

A new modeling approach was developed to test the hypothesis for the causes of the observed oxygen variability. We constructed a three-dimensional numerical model of oxygen anomaly driven by the data-constrained circulation fields from the GECCO dataset. In the calculation, the effect of air-sea gas exchange and biological variability is suppressed such that the simulated oxygen anomaly is solely driven by the circulation variability. Simulated oxygen variability captures many aspect of the observed oxygen at OSP (correlation coefficient between model and observation is 0.75). The Gulf of Alaska is a hot spot of oxygen variability with an elevated standard deviation. We conducted an EOF analysis on simulated oxygen over the North Pacific, and found that more than 50% of variance of thermocline oxygen is explained by the first two EOF in the extratropical North Pacific. The first PC of thermocline oxygen is significantly correlated with the second PC of SST (correlation coefficient is 0.7) associated with the North Pacific Oscillation (NPO) and the second PC of thermocline oxygen is significantly correlated

with the first PC of SST (correlation coefficient is 0.5) associated with the Pacific Decadal Oscillation (PDO). The circulation pattern associated with oxygen variability involves the north-south dipole in the barotropic streamfunction. Thus the dominant mode of the oxygen anomaly over the North Pacific can be well explained by the modes of climate variability in the North Pacific, namely PDO and NPO. The oxygen budget analysis for region around the OSP shows the importance of the role of horizontal advection. In summary, the large-scale climate variability and associated ocean circulation fluctuations can generate oxygen anomalies in the thermocline. Our analysis revealed that this climate-driven oxygen anomaly can explain significant fraction of observed oxygen changes in the subpolar North Pacific. There is a clear and strong link between the leading EOFs of thermocline oxygen and the dominant modes of SST variability.

There are many caveats and remaining questions left for future study. We have not yet examined the statistics over the seasonal timescale due to the sparse sampling density after 1980s. It may be possible to separate the data into warm and cold seasons and conduct statistical analysis to examine the role of seasonality, which is left for future study. Extracting low-frequency and high-frequency component of the time series using some filtering method may also be another approach to see the detailed features of low and high frequency variability. Further study is necessary to systematically understand the mechanism where climate variability influences biogeochemical tracers through modulating air-sea interaction, biological productivity as well as circulation changes. This will require model refinements in both physical circulation as well as parameterization of marine ecosystem, generation and remineralization of particulate

organic matter and cycling of elements in the upper ocean, which are active areas of research. Due to its strong sensitivity of climate, dissolved oxygen in the ocean thermocline can be a useful tracer to test the performance of future generations of ocean circulation and biogeochemistry models.

BIBLIOGRAPHY

- [1] Bretherton, C. S., M. Widmann, V. P. Dymnikov, J. M. Wallace, and I. Blade (1999), The effective number of spatial degrees of freedom of a time varying field. *J. Climate*, 12:1990–2009.
- [2] Cummins, PF. and G. S. E. Lagerloef (2002), Low-frequency pycnocline depth variability at ocean weather station P in the northeast Pacific. *J. Phys. Oceanogr.* 32:3207–3215.
- [3] Davis, J (1975), Minimal dissolved oxygen requirements of aquatic life with emphasis on Canadian species: a review. *Journal of the Fisheries Research Board of Canada* 32, 2295–2332.
- [4] Deutsch, C., S. Emerson, and L. Thompson (2005), Fingerprints of climate change in North Pacific oxygen, *Geophys. Res. Lett.*, 32, L16604, doi:10.1029/2005GL023190.
- [5] Deutsch, C., S. Emerson, and L. Thompson (2006), Physical-biological interactions in North Pacific oxygen variability, *J. Geophys. Res.*, 111, C09S90, doi:10.1029/2005JC003179.
- [6] Di Lorenzo, E. et al. (2008), North Pacific Gyre Oscillation links ocean climate and ecosystem change, *Geophys. Res. Lett.*, 35, L08607, doi:10.1029/2007GL032838.
- [7] Emerson, S., Y. W. Watanabe, T. Ono, and S. Mecking (2004), Temporal trends in apparent oxygen utilization in the upper pycnocline of the North Pacific: 1980– 2000, *J. Oceanogr.*, 60, 139–147.
- [8] Garcia, H. E., et al. (2006), *World Ocean Atlas 2005, Volume 3: Dissolved Oxygen, Apparent Oxygen Utilization, and Oxygen Saturation*. S. Levitus, Ed. NOAA Atlas NESDIS 63, U.S. Government Printing Office, Washington, D.C., 342 pp
- [9] Gent P. R., and J. C. McWilliams (1990), Isopycnal mixing in ocean circulation models. *J. Phys. Oceanogr.*, 20, 150-155.
- [10] Gray, J.S., Wu, R.S., Or, Y.Y (2002) Effects of hypoxia and organic enrichment on the coastal marine environment. *Marine Ecology Progress Series* 238, 249–279.
- [11] Hasselmann, K. (1976), Stochastic climate models. 1. Theory, *Tellus*, 28(6), 473–485.
- [12] Ito, T., M. Follows, and E. A. Boyle (2004), Is AOU a good measure of respiration in the oceans?, *Geophys. Res. Lett.*, 31, L17305, doi:10.1029/2004GL020900.

- [13] Ito T. and C. Deutsch (2010), A conceptual model for the temporal spectrum of oceanic oxygen variability, *Geophys. Res. Lett.* 37, L03601, doi:10.1029/2009GL041595.
- [14] Keeling, R. F., and H. E. Garcia (2002), The change in oceanic O₂ inventory associated with recent global warming, *Proc. Natl. Acad. Sci. U. S. A.*, 99(12), 7848–7853, doi:10.1073/pnas.122154899.
- [15] Keeling, R. F., A. Kortzinger, and N. Gruber. *Ocean* (2010), Deoxygenation in a Warming World. *Annual Review of Marine Science*, Vol. 2: 199-229, 2010 doi:10.1146/annurev.marine.010908.163855.
- [16] Köhl, A., et al. (2006), The Global ECCO 1952 to 2001 Ocean Synthesis, The ECCO Report Series No.40.
- [17] Large, W. G., J. C. McWilliams, and S. C. Doney (1994), Oceanic Vertical Mixing - a Review and a Model with a Nonlocal Boundary-Layer Parameterization, *Rev Geophys*, 32(4), 363-403.
- [18] Linkin, M. E., and S. Nigam (2008), The North Pacific Oscillation--West Pacific teleconnection pattern: Mature-phase structure and winter impacts. *J. Climate*, 21, 1979 - 1997.
- [19] Mantua, N.J. and S.R. Hare, Y. Zhang, J.M. Wallace, and R.C. Francis (1997) A Pacific interdecadal climate oscillation with impacts on salmon production. *Bulletin of the American Meteorological Society*, 78, 1069-1079.
- [20] Marshall, J., C. Hill, L. Perelman, and A. Adcroft (1997), Hydrostatic, quasi-hydrostatic, and nonhydrostatic ocean modeling, *J. Geophysical Res.*, 102(C3), 5733-5752.
- [21] Marshall, J., A. Adcroft, C. Hill, L. Perelman, and C. Heisey (1997), A finite-volume, incompressible Navier Stokes model for studies of the ocean on parallel computers, *J. Geophysical Res.*, 102(C3), 5753-5766.
- [22] Marotzke, J., R. Giering, K. Q. Zhang, D. Stammer, C. Hill, and T. Lee (1999), Construction of the adjoint MOT ocean general circulation model and application to Atlantic heat transport sensitivity, *J. Geophys. Res.*, 104, 29,529– 29,547.
- [23] Najjar, R. G., J. L. Sarmiento and J. R. Toggweiler, (1992), Downward transport and fate of organic matter in the ocean: Simulations with a General Circulation model, *Global Biogeochem. Cycles*, 6, 45-76.

- [24] Ono, T., T. Midorikawa, Y. W. Watanabe, K. Tadokoro, and T. Saino (2001), Temporal increases of phosphate and apparent oxygen utilization in the subsurface waters of western subarctic Pacific from 1968 to 1998, *Geophys. Res. Lett.*, 28(17), 3285– 3288, doi:10.1029/2001GL012948.
- [25] Walker, G. T., and E. W. Bliss (1932), *World weather V. Mem. Roy. Meteor. Soc.*, 4, 53–84.
- [26] Watanabe, Y. W., M. Shigemitsu, and K. Tadokoro (2008), Evidence of a change in oceanic fixed nitrogen with decadal climate change in the North Pacific subpolar region, *Geophys. Res. Lett.*, 35, L01602, doi:10.1029/2007GL032188.
- [27] Whitney, F.A., Freeland, H.J (1999), Variability in upper-ocean water properties in the NE Pacific Ocean. *Deep-Sea Research II* 46, 2351–2370.
- [28] Whitney, F. A., H. J. Freeland, and M. Robert (2007), Persistently declining oxygen levels in the interior waters of the eastern subarctic Pacific, *Prog. Oceanogr.*, 75(2), 179–199, doi:10.1016/j.pocean.2007.08.007.
- [29] Wunsch, C., and P. Heimbach (2007), Practical global oceanic state estimation, *Physica D: Nonlinear Phenomena*, 230(1-2), 197-208.